Geological Magazine

www.cambridge.org/geo

Cryogenian-Ediacaran crustal growth and evolution of the active margin of the Dahomeyide belt, Ghana

Daniel Kwayisi[1,2], Emmanuel Nyavor[2], Elikplim Abla Dzikunoo[2], Iris Ekua Mensimah Fynn[3], Jacob Kutu[2] and Prosper M Nude[2]

[1]Department of Geology, University of Johannesburg, Auckland Park Kingsway Campus, South Africa; [2]Department of Earth Science, University of Ghana, Legon-Accra, Ghana and [3]Department of Geography and Resource Development, University of Ghana, Legon-Accra, Ghana

Original Article

Cite this article: Kwayisi D, Nyavor E, Dzikunoo EA, Fynn IEM, Kutu J, and Nude PM. Cryogenian-Ediacaran crustal growth and evolution of the active margin of the Dahomeyide belt, Ghana. *Geological Magazine* https://doi.org/10.1017/S0016756823000808

Received: 19 September 2023
Revised: 1 December 2023
Accepted: 4 December 2023

Keywords:
crustal thickening; crustal anatexis; continent-continent collision; migmatite; continental subduction

Corresponding author:
Daniel Kwayisi; Email: danielk@uj.ac.za

Abstract

The study presents detailed petrographical, geophysical, structural and geochemical data of the internal nappes zone to establish the deformational history, origin and tectonic setting and constrain the crustal growth and evolution of the active margin of the Dahomeyide belt. Two main lithological units, (i) deformed meta-granitoids (migmatites and gneisses) and (ii) undeformed granitoids, dominate the internal nappes zone. The granitoids are generally I-type, metaluminous to weakly peraluminous, low-K tholeiite to high-K calc-alkaline and of tonalite, granodiorite and granite affinity. The overall trace element patterns of the studied granitoids characterized by the enriched LILE and depleted HFS, with negative peaks of Nb-Ta, Sr, P and Ti, are indications of arc-related magmatism. Structural analysis reveals four deformation phases (D_1-D_4). D_1 represents Northwest-Southeast (NW-SE) Pan African shortening associated with a continent-continent collision, resulting in westward nappe stacking. Progressive NW-SE shortening resulted in D_2 and D_3 top-to-the-NW dextral and sinistral thrusting events during the Pan-African orogeny. D_4 is an extensional event likely associated with the orogenic collapse phase. The gneisses and migmatites, with dominant axial planar foliations, point to their formation in a collisional setting or influence by the Pan-African collisional processes. Continental-arc signatures in these rocks imply continental subduction during their protolith formation. The intrusive granitoid and pegmatite are undeformed, meaning late- to post-orogenic emplacement. These findings suggest that the internal nappes zone archived the subduction-collision and post-collisional phase of the Pan-African orogeny and recorded large-scale migmatization and granitoid emplacement due to partial melting of thickened lower crust between Mid-Cryogenian and late Ediacaran.

1. Introduction

The Pan-African Dahomeyide belt occupying the southeastern margin of the West African Craton records a complete orogenic cycle during the Cryogenian-Ediacaran period and consists of features, including basement complex, passive margin, oceanic terrane and active margin (arc-crust and post-collisional basins) (Figure 1(a) and (b); Attoh and Nude, 2008; Attoh et al. 2013; Aidoo et al. 2021; Kwayisi et al. 2022*a*). The Dahomeyide belt forms the central segment of the West Gondwana Orogen (inset Figure 1(a)) and formed during the subduction-collision phases of the Pan-African orogeny (Attoh and Nude, 2008; Guillot et al. 2019; Aidoo et al. 2021). Based on lithology and tectonics, this belt has been divided into an internal nappes zone, suture zone and external nappes zones (Duclaux et al. 2006; Attoh and Nude, 2008; Kwayisi et al. 2020). In a plate tectonic scenario, the upper and lower plates of the Dahomeyide belt are represented by the internal and external nappes zones, respectively (Figure 1(c)), and separated by a well-defined suture zone of ultrahigh pressure-high pressure eclogite and granulite rocks (Figure 1(b) and (c); Attoh and Morgan, 2004; Attoh and Nude, 2008). The internal nappes zone (Figure 1(b) and (c)) corresponds to the active margin of the Dahomeyide belt that recorded arc-related and post-collisional magmatism and intracontinental extensional volcanism and sedimentation during the Pan-African orogeny (Kalsbeek et al. 2012; Attoh et al. 2013; Ganade de Araujo et al. 2016). The internal nappes zone is made up of granitoids and supracrustal rocks formed due to the east-dipping subduction and continent-continent collision between the West African Craton and the Benin-Nigerian Shield (BNS) and extensional-related volcanic and sedimentary rocks formed after collision (e.g., Attoh and Nude 2008; Attoh et al. 2013; Ganade de Araujo et al. 2016; Guillot et al. 2019). The granitoids constitute the bulk of the internal nappes zone, with the supracrustal and extensional-related rocks being only minor (Kalsbeek et al. 2012; Attoh et al. 2013; Ganade de Araujo et al. 2016).

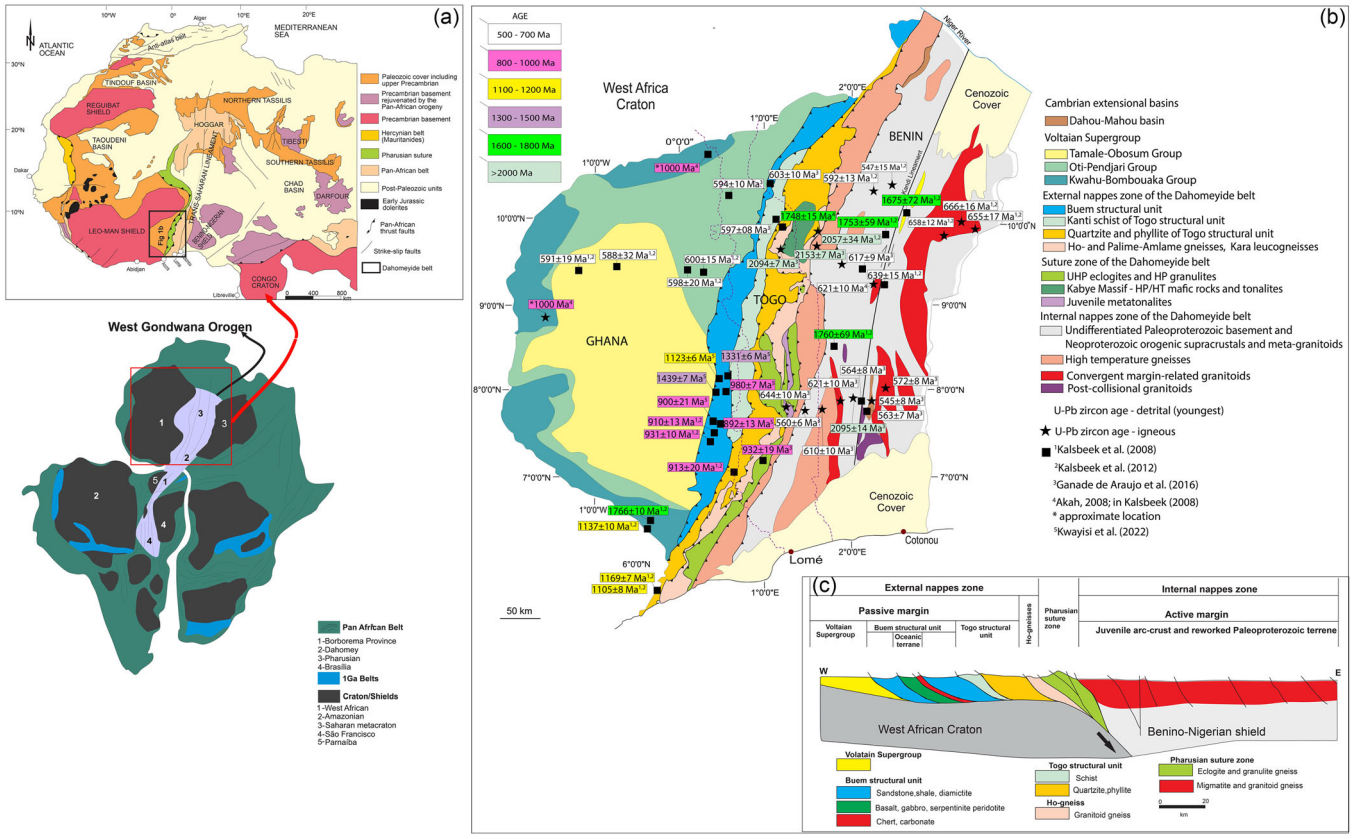

Figure 1. (Colour online) (a) Schematic geological map of the West African Craton (insert is the map of West Gondwana Orogen; after Ganade de Araujo et al. 2016), (b) Geological map of Dahomeyide belt (modified after Kwayisi et al. 2022*b*), (c) Cross-section of the Dahomeyide belt, showing the lower plate (i.e., external nappes zone, to the west), upper plate (internal nappes zone (Active margin), to the east), separated by the suture zone (modified after Guillot et al. 2019).

Two major types of granitoids occur in the internal nappes zone of the Dahomeyide belt. (i) migmatites, and (ii) gneisses (Table 1: Attoh et al. 2013) intruded by granites and granodiorites (Kalsbeek et al. 2012; Attoh et al. 2013). Kalsbeek et al. (2012) obtained U-Pb zircon ages of 547 ± 15 Ma and 666 – 592 Ma for the intrusive granitoids and the migmatites, respectively. Similarly, U-Pb ages of 620 – 589 Ma have been obtained for the migmatites by Attoh et al. (2013). The 589 – 547 Ma age corresponds to post-collisional magmatism, with the 666 – 620 Ma corresponding to arc-related magmatism (Kalsbeek et al. 2012; Attoh et al. 2013; Ganade de Araujo et al. 2016). These ages suggest an approximately 100 Ma span of arc-related and post-collisional magmatism during the Pan-African orogeny between Mid-Cryogenian at 670 and late Ediacaran at 540 Ma (Kalsbeek et al. 2012).

Very little is known about the structural evolution of the granitoids of the internal nappes zone (i.e., active margin) of the Dahomeyide belt in Ghana. Hence, it becomes difficult to interpret the tectonic evolution of these units in relation to the Pan-African orogeny. However, elsewhere in the Parakou-Nikki region of northern Benin, five deformational phases have been interpreted and linked to various stages of the Pan-African orogeny (Chala et al. 2015). This work, therefore, seeks to shed light on the structural evolution by integrating field, geophysical and structural data of the Dahomeyide internal nappes zone and examine their significance in the overall crustal growth and evolution of the Dahomeyide belt and implications to the Pan-African orogeny. Besides, there is no petrographical and geochemical data on the post-collisional granitoids to constrain their source, tectonic setting and petrogenetic evolution. Hence, the major and trace element concentration of the post-collisional granitoids and also new geochemical data of the arc-related granitoids (i.e., the gneisses and migmatites) are presented to infer their source, tectonic setting and petrogenetic evolution.

2. Geological setting

The internal nappes zone (i.e., active margin) of the Pan-African Dahomeyide belt represents the south-western portion of the Benin-Nigerian Shield, which is the south-western limit of the Saharan metacraton (Figure 1(a); Abdelsalam et al. 2002; Chala et al. 2015). The other zones of the Pan-African Dahomeyide belt are the external and the suture zones (Guillot et al. 2019; Kwayisi et al. 2020; 2022*b*). The external nappes zone represents the lower plate, whereas the internal nappes zone is the upper plate of the Pan-African Dahomeyide belt. The suture zone is the vestiges of the Pharusian oceanic crust, formed during the Pan-African oceanic accretionary phase (Duclaux et al., 2006; Attoh and Morgan, 2004; Agbossoumondé et al. 2017; Kwayisi et al. 2022*a*). The internal nappes zone occurs to the immediate east of the suture zone, where they are separated by tectonic contacts (Figure 1(b)). The internal nappes zone is made up of a complex of meta-granitoid basement, underlying volcano-sedimentary Neoproterozoic supracrustals, and invaded by several generations of arc-related Pan-African and post-collisional granitoids (Table 1; Figure 1(b); Affaton et al. 1991; Attoh et al. 2013; Ganade de Araujo et al. 2016). Attoh et al. (2013) subdivided the meta-granitoid basement of the internal nappes

https://doi.org/10.1017/S0016756823000808 Published online by Cambridge University Press

Table 1. Compiled lithological, metamorphic, P-T, age and tectonic data on the internal nappes zone of the Dahomeyide belt

Unit		Metamorphism	P-T condition	Crystallization/ depositional age	Metamorphic age	Setting
Granitoid gneiss and migmatite*	Biotite bearing migmatite*	Amphibolite facies‡	”	666 – 592 Ma*,§ (U-Pb, zircon)	”	Magmatic arc*
	Hornblende ± garnet-bearing dioritic gneiss*			2190–2140 Ma*,‖ (U-Pb, zircon)		
Supracrustal rocks†	Schist†	”	”	600 Ma† (U-Pb, zircon, detrital)	”	Foreland†
	Migmatite†			660 Ma† (U-Pb, zircon, detrital)		
	Quartzite†					
Extensional volcanic and sedimentary rocks†	Dacite†			545.7 ± 7.8 Ma† (U-Pb, zircon)		Post collision extensional rifting*
	Conglomeratite†			563 ± 7 Ma† (U-Pb, zircon, detrital)		

*Attoh et al. (2013).
†Ganade de Araujo et al. (2016).
‡Nude (1995).
§Kalsbeek et al. (2012).
‖Kalsbeek et al. (2020).

zone into two, namely dioritic gneiss, characterized by hornblende as the main mafic mineral and occasional garnet and migmatite with biotite as the dominant mafic mineral (Table 1). U-Pb zircon ages of 666 – 620 Ma corresponding to arc-related magmatism have been obtained for the migmatites (Figure 1(b); Kalsbeek et al. 2012; Attoh et al. 2013; Ganade de Araujo et al. 2016). The migmatites have been postulated as juvenile crust representing the arc terrane that formed due to subduction and oceanic closure during the Pan-African orogeny (Attoh et al. 2013). However, older U-Pb zircon crystallization ages ranging from 2.14 to 2.19 Ga were recorded for the dioritic gneisses (Attoh et al. 2013). The Paleoproterozoic ages signify the involvement of older crust (Saharan Metacraton), representing the basement of the Benin-Nigerian Shield, in the Pan-African Dahomeyide belt (Duclaux et al. 2006; Attoh et al. 2013). The migmatites are intruded by post-collisional granitoids dated at 589 – 547 Ma, corresponding to post-collisional magmatism (Kalsbeek et al. 2012; Attoh et al. 2013).

3. Field relations and petrography

Field observations and petrographical investigations reveal that two main lithological units dominate the internal nappes zone of southeastern Ghana. These are (i) deformed meta-granitoids made up of migmatites and gneisses and (ii) undeformed granitoids, herein referred to as intrusive granitoids composed dominantly of granite and minor granodiorite. Amphibolite, pegmatite, aplite and quartz veins also occur. Figure 2 is a geological map of southeastern Ghana, showing the extent and distribution of the rocks in the study area. The deformed meta-granitoids dominate over the intrusive granitoids in terms of volume. Widespread in the internal nappes zone are the migmatites (Figure 2).

In general, the migmatite consists of alternating leucosomes and melanosomes, thus representing typical stromatic migmatite (Figure 3(a)). The migmatite is coarse-grained and contains microcline (45%), quartz (30%), plagioclase (15%), biotite (7%), muscovite (2%) and garnet (1%), with epidote, titanite, zircon and rutile as accessory minerals. This rock shows micro-folds defined by bent quartz grains (Figure 3(b)). Myrmekites of K-feldspar in plagioclase are present as small spots disseminated in some plagioclases or invading K-feldspar and plagioclase from their margins (Figure 3(c)). The gneisses are made up of felsic augen, biotite and hornblende-biotite gneisses. The felsic augen gneiss shows coarse-grained augen feldspars in a porphyroblastic texture (Figure 3(d)). Generally, the rock appears light grey with a porphyroblastic and myrmekite texture. It consists of quartz (30%), plagioclase (25%), orthoclase (15%), microcline (15%), biotite (12%), hornblende (2%) and sericite (1%) in a preferred orientation (Figure 3(e)). The porphyroblasts are essentially orthoclase. In contrast, biotite occurs as interstitial or inclusions in orthoclase. Inclusions of quartz occur in the microcline and orthoclase, while sericite occurs as inclusions or secondary minerals in the plagioclase and microcline. The biotite gneiss (Figure 3(f)) has a coarse-grain texture and well-defined foliations. This rock consists of quartz (40%), microcline (25%), plagioclase (20%), biotite (10%), muscovite (4%), sericite (1%) and accessory phases, including titanite, zircon and garnet (Figure 3(g)). Garnet contains inclusions of quartz and micro-fractures, filled with elongate biotite. The hornblende-biotite gneiss has a coarse-grain texture and a pale ash-grey colour (Figure 3(h)). It consists of plagioclase (33%), quartz (20%), orthoclase (20%), biotite (15%), hornblende (5%), microcline (3%), garnet (2%) and calcite (1%) with accessory muscovite and epidote (Figure 3(i)). Inclusions of quartz and muscovite occur in the plagioclase.

Within the internal nappes zone, but distinctly different from the typical deformed migmatites and gneisses, are intrusive bodies of granitic and granodioritic rocks (intrusive granitoids) with sharp lithological boundaries with the migmatites and gneisses (Figures 4(a) and (b)). They are distinguished by being typically undeformed or only weakly deformed. The granite occurs as large and massive bodies within the biotite gneiss (Figure 4(a)), whereas the granodiorite occurs as a dyke within the migmatite and felsic

https://doi.org/10.1017/S0016756823000808 Published online by Cambridge University Press

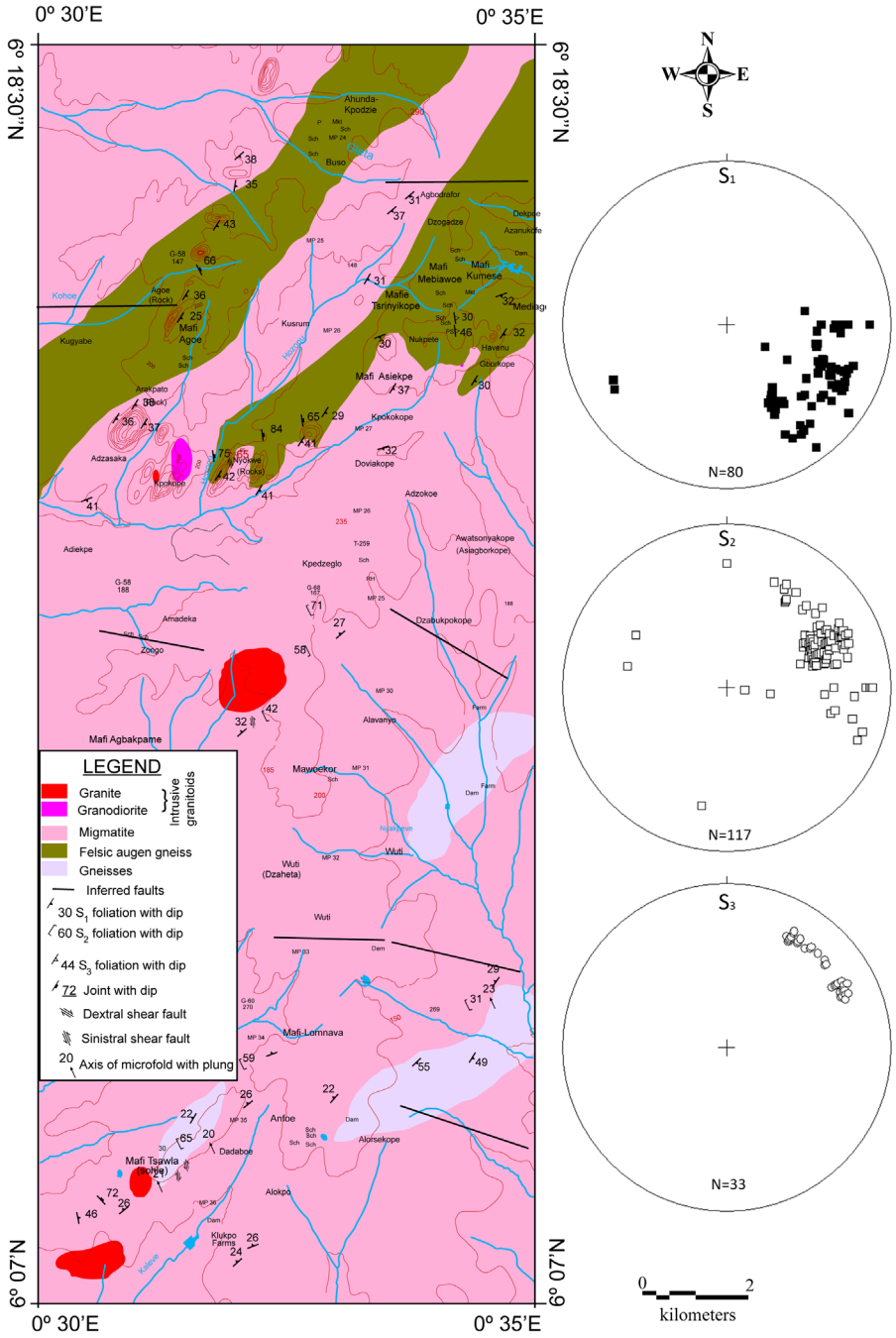

Figure 2. (Colour online) Geological map of southeast Ghana showing the lithological distribution and structural relationships of the rocks of the study area. Insert are the pole to plane plots of the S_1, S_2 and S_3 foliations.

augen gneiss, generally oriented north-south and discordant to the general foliations of the host rock (Figure 4(b)). The granite (Figure 4(c)) is leucocratic, characterized by phaneritic texture, and consists of microcline (45%), quartz (25%), plagioclase (20%), biotite (6%), muscovite (2%), sericite (2%), epidote (1%) and garnet occurring as accessory minerals. Micro-fractures occur in the quartz, biotite inclusions in the microcline and quartz in plagioclase. Muscovite and sericite are secondary minerals derived from the alteration of feldspars. The granodiorite is medium to coarse-grained with characteristic myrmekitic textures. It consists of quartz (30%), plagioclase (25%), biotite (15%), orthoclase (12%), hornblende (12%), calcite (4%) and microcline (2%) (Figure 4(d)). Some of the quartz grains occur as minor fine inclusions in the plagioclase, hornblende and biotite.

4. Structures and deformation

The structural elements of the Dahomeyide internal nappes zone of southeastern Ghana are characterized by four deformational events (D_1, D_2, D_3, and D_4), which are well-developed in the gneisses and migmatites. An earlier D_1 phase formed NE-SW S_1 foliations and asymmetric quartz porphyroblasts and was associated with F_1 isoclinal folds (Figures 5(a) and (b)). The plot to poles for the S_1 foliations also shows that the foliations generally dip to the southeast and are concentrated closer to the sphere than the centre and, therefore, indicate low to moderate dip angles to the southeastern direction (Figure 2).

D_2 phase corresponds to the formation of S_2 foliations (NW-SE striking cleavages), F_2 folds (drag folds), kink folds and coeval with penetrative top-to-the-NW dextral (C-S fabrics) shear plane (C_2)

https://doi.org/10.1017/S0016756823000808 Published online by Cambridge University Press

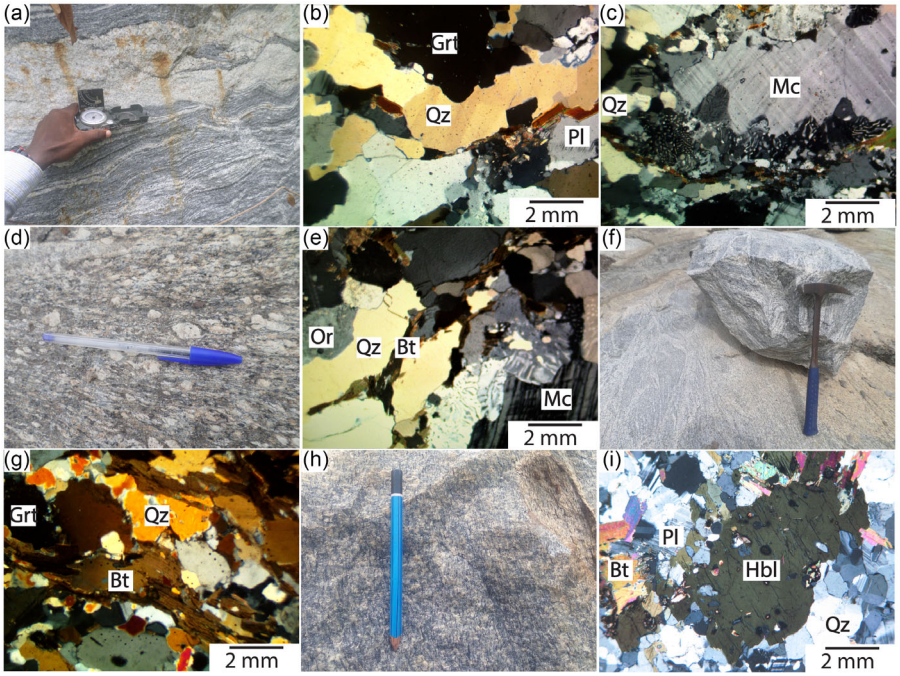

Figure 3. (Colour online) Field photos and photomicrographs of the gneisses and migmatite of the internal nappes zone (a) Migmatite consists of alternating leucosomes and melanosomes, thus representing typical stromatic migmatite, (b) Migmatite showing micro-folds defined by bent quartz grains (crossed polars), (c) Myrmekite texture invading microcline and plagioclase at their margins, (d) Felsic augen gneiss with coarse-grained augen feldspars (crossed polars), (e) Foliation in the felsic augen gneiss defined by elongated quartz and biotite (crossed polars), (f) Biotite gneiss with phaneritic texture and well-defined foliations, (g) Foliation in biotite gneiss defined by biotite minerals (crossed polars), (h) Hornblende-biotite gneiss and (i) Hornblende-biotite gneiss with coarse hornblende minerals (crossed polars). Bt = biotite, Grt = garnet, Hbl = hornblende, Mc = microcline, Or = orthoclase, Pl = plagioclase, Qz = quartz. Mineral abbreviation is from Whitney and Evans (2010).

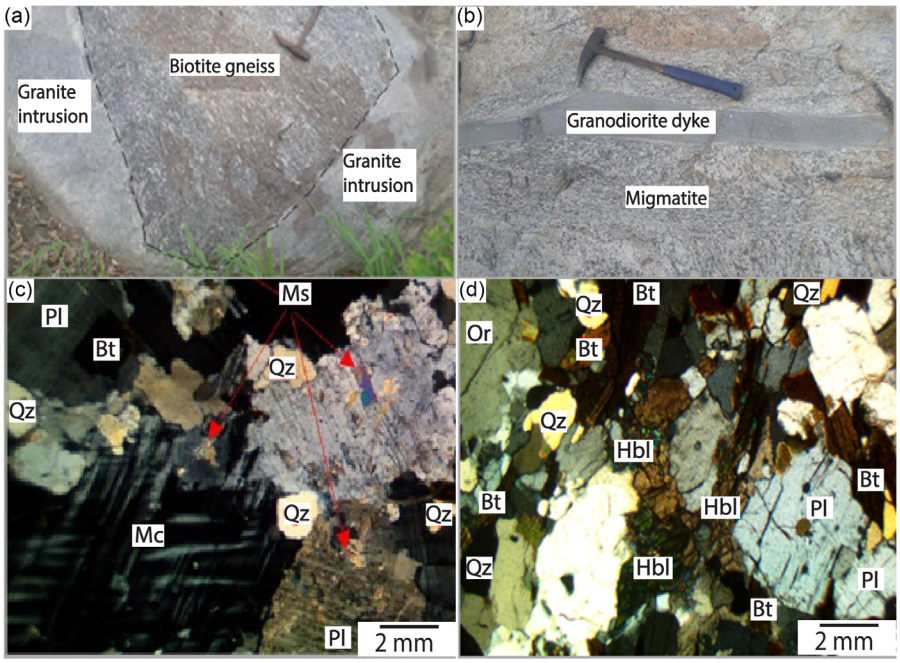

Figure 4. (Colour online) Field photos and photomicrographs of the intrusive bodies of the internal nappes zone. (a) Large intrusion of granite bodies into the biotite gneiss, (b) Dykes of granodiorite within the migmatite (c) Leucocratic granite characterized by phaneritic texture (crossed polars) and (d) Granodiorite showing medium to coarse-grained with characteristic myrmekitic textures (crossed polars).

as well as the formation of older generational joints in the gneisses and migmatites (Figures 2, 5(a) and (c)–(e)). The stereographic projections (plot to pole) of these planes show a general concentration close to the centre of the circle, indicating moderate to high dips for the cleavages (Figure 2). The presence of kink folds is also an indication of the high intensity of the D_2 event. The D_2 event also produced small-scale Z-shaped drag and parasitic folds.

D_3 event is a shearing event with a top-to-the-NW sinistral (C-S fabric) shear plane (C_3; Figures 2 and 5(f))). These small-scale faults are observed only in the migmatites and gneisses. The C_3 shear fault planes generally strike in the NW-SE directions with low to moderate dips to the southwest. The C_3 faults displaced S_1 foliations, the C_2 dextral shear faults, the F_2 folds and the older joints and developed the low NNE dipping S_3 foliations (Figure 2).

A final D_4 event resulted in the formation of the younger generational joint and fault planes striking in East-West (E-W) and Northnorthwest-Southsoutheast (NNW-SSE) directions (Figure 5(f)). The effects of this deformation are observed in the aplite veins and granodiorite dyke.

https://doi.org/10.1017/S0016756823000808 Published online by Cambridge University Press

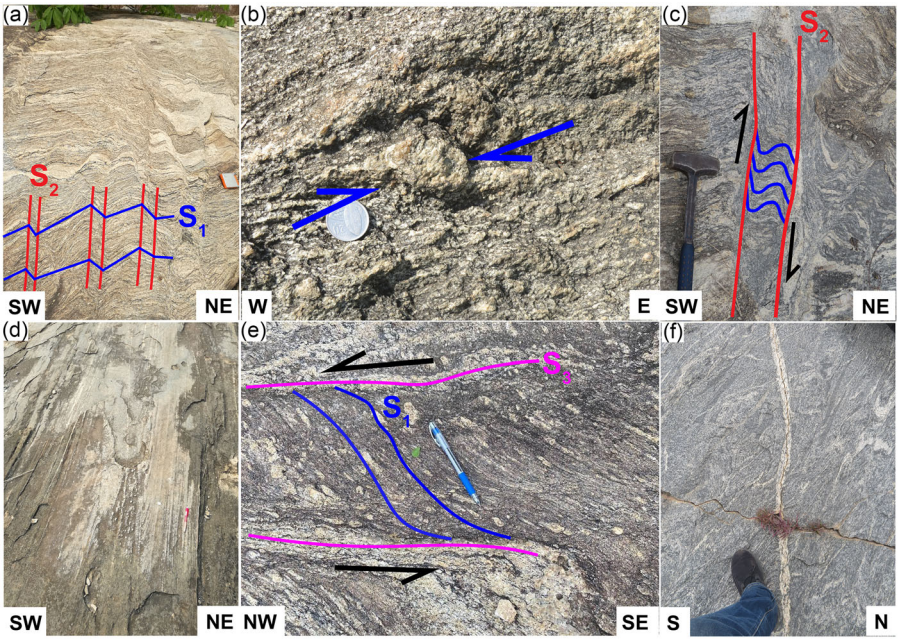

Figure 5. (Colour online) (a) Northeast-Southwest (NE-SW) S_1 foliations in the migmatite folded by F_2 kink folds (b) Quartz porphyroblasts showing top-to-the-NE shearing, (c) F_2 fold (drag folds), and penetrative top-to-the-NW dextral (C-S fabrics) shear plane (C_2) (d) Near horizontal NW-dipping L_2 stretching lineation, (e) C_3 sinistral top-to-the-NW shear (C-S fabrics) planes with generally NW-SE strike and (f) Late joints cutting through the migmatite and some veins. Most of the outcrops occur as platforms thus, features were viewed on the horizontal surface.

5. Geophysical data processing and interpretation

5.1. Geophysical data processing

The aeromagnetic geophysical survey data for the study area was obtained from the Ghana Geological Survey Authority, Accra. This data was acquired between February and November 1997 by the Geological Survey of Finland. The survey was flown in the E-W direction with a nominal line separation set at 400 m and a terrain clearance of 70 m. The data was grid using the bi-directional gridding method because it strengthens trends perpendicular to the survey line directions. The disadvantage, however, is that tie-line data cannot be incorporated into the interpolation method.

The total magnetic intensity grid (TMI) obtained from the gridding was enhanced by applying appropriate filters such as reduce to the equator (RTE), first vertical derivative (1VD), tilt derivative (TD) and automatic gain control (AGC). The RTE filter was applied on the TMI grid to reposition anomalies directly over their sources (Milligan and Gunn, 1997; Kwayisi et al. 2020; Dzikunoo et al. 2021). The RTE was chosen over the reduced to-pole because of the study area's low latitude position. An inclination of −13.17 and a declination of −5.23 were applied in the filtering; the final result was then inverted using a multiplication factor of −1.

Akin to the RTE operation, the analytic signal (AS) centres anomalies directly over causative bodies (Gunn, 1997). Additionally, it is useful in low magnetic latitudes because of its independence from ambient fields and the direction of source body magnetization (Gunn, 1997). Ridges or peaks in the AS-TMI anomaly map coincide with faults, shear zones and lithological contacts. The 1VD filter was applied to the RTE grid to enhance shallow geological structures by accentuating short-wavelength (high wave-number) anomalies that are caused by surface and near-surface geological bodies (Paine, 1986). The 1VD filter also enhances the edges of anomalies to determine the boundaries of geological bodies easily. This filter allows for the visualization of the change in the measured parameters as distance to source (survey height) changes. It is ideal to perform the 1VD filter on the RTE-TMI grid because the output will show the zero contour values directly over the edges of the magnetic source bodies (Kwayisi et al. 2020; Dzikunoo et al. 2021).

The AGC and TD were applied on the RTE grid. The AGC works to enhance minor structural trends, making them more discernible. Its application works with some rescaling applications to reduce the dynamic range of magnetic data to avoid substantial anomalies and mask subtle anomalies. The TD, conversely, defines the extent of the edges of the various sources (Oruc and Selim, 2011). The enhancement highlights short wavelengths. The processed geophysical maps were opened in an ArcGIS environment for detailed interpretation. Geophysical maps were used to identify lineaments, which include folds, faults and thrusts. This was done by observing certain characteristics such as displacement in a noticeable linear feature, a sudden change in amplitude, duplication of magnetic signals, truncation of a primarily linear magnetic domain by a curvilinear feature and a curved magnetic pattern (Kwayisi et al. 2020).

5.2. Geophysical data interpretation

The TMI map shows a sort of division of magnetic intensities, with the area to the north showing higher magnetic intensities than the area to the south (Figure 6(a)). The RTE shows a similar distribution of the magnetic signatures with a better definition of some features. The RTE grid was then inverted (Figure 6(b)), giving high anomalies the appropriate pink colour for straightforward interpretation and comparison. The general NE-SW feature trend is likely related to the S_1 NE-SW foliations observed on the field (Figures 2, 6(a) and (b)).

The AS map and the RTE-inv both show a central NE-SW trending region with high magnetic anomalies and traces of structures (Figures 6(b) and (c)). The NNE-facing nose of a tight chevron fold is seen at the southwesternmost end of the study area and within the demarcated shear zone (Figure 6(d)). This is linked to F_1 folding event that resulted in the NE-SW S_1 foliation. A major thrust/shear plane runs through the central portion of the study area (Figure 6(d)). The thrusting is observed as a repetition of the magnetic anomalies. These observed thrust/shear depict top-to-the-

https://doi.org/10.1017/S0016756823000808 Published online by Cambridge University Press

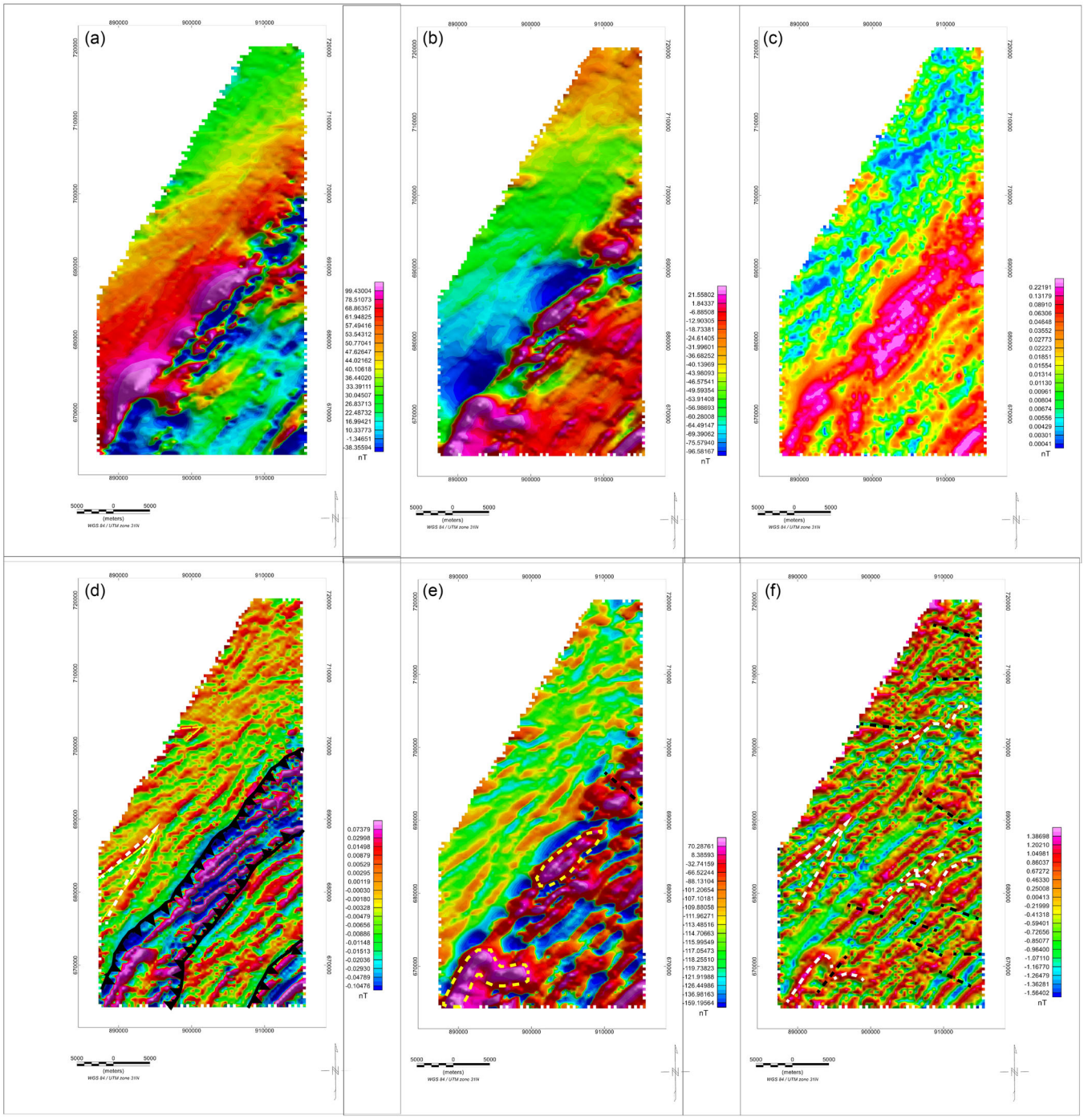

Figure 6. (Colour online) (a) Total Magnetic Intensity map of the internal nappes zone of the Dahomeyide belt with NE-SW striking high and low magnetic intensities corresponding to different geological terrains, (b) Inverted Reduced-to-the-equator map of the internal nappes zone, giving high anomalies the appropriate pink colour for straightforward interpretation and comparison, (c) Analytic signal map that is useful in centring anomalies directly over causative bodies, and showing NE-SW trending region with high magnetic anomalies and traces of structures and (d) First Vertical Derivative map showing major thrust faults as a result of cyclic map repetition of the same magnetic signal. (e) Automatic gain control map exhibiting intermittent high and low magnetic signatures in the mid-portion and southeastern corner of the study area. These correspond to biotite gneiss and intrusive granitoids, and (f) dominantly NW-SE striking and few E-W striking faults and joints are observed on the Tilt derivative map.

NW movement and thus may be associated with both dextral strike-slip and sinistral strike-slip movement of D_2 and D_3 events. In fact, observed dextral and sinistral fault plane falls within this zone (Figure 2). The dextral strike-slip and sinistral strike-slip movements are thus, related to D_2 and D_3 deformational events that developed the C_2 and C_3 shear planes, respectively, observed in the field (Figure 5).

Lithologically, biotite gneiss and intrusive granitoid (granite and granodiorite) rocks seem to occupy the shear zone with some enclaves of garnet amphibole gneiss (Agyei-Duodu et al. 2009). These exhibit intermittent high and low magnetic signatures in the mid-portion and southeastern corner of the study area in the AGC map (Figure 6(e)). Late dominantly NW-SE striking and few E-W striking faults and joints are observed

https://doi.org/10.1017/S0016756823000808 Published online by Cambridge University Press

on the TD map (Figure 6(f)). These late faults and joints correspond to the late D_4 deformational event observed in the field.

6. Geochemical characteristics

6.1. Analytical procedure

Representative samples of migmatites (3), gneisses (8), intrusive granitoids (5) and pegmatite (1) were analyzed for major and trace element concentrations at the ALS laboratory in Vancouver, Canada. Analytical techniques followed the protocol of the procedures at the ALS laboratory (see Kwayisi et al. 2017). The major and trace elements analyses were carried out by Inductively Coupled Plasma-Atomic Emission Spectrometry and multi-elements fusion Inductively Coupled Plasma Mass Spectrometry, respectively. Loss on ignition was determined at 1000°C. Elements with concentration >1 wt. % recorded 1 – 3% analytical uncertainty, whereas those in low concentrations (<1 wt. %) recorded uncertainty of 10%. On the whole, precision was better than 5%.

6.2. Major and trace element concentrations

Major and trace element concentrations for representative samples of the granitoids of the internal nappes zone (i.e, active margin) of the Dahomeyide belt are presented in Table 2. The gneisses vary in terms of their major element concentrations. The biotite-hornblende gneiss has the lowest SiO_2 (63.6 – 66.5 wt. %) content, followed by the biotite gneiss (SiO_2 = 69.1 – 70.8 wt. %) with the felsic augen gneiss having the highest SiO_2 (76.2 wt. %) content. However, the concentrations of the ferromagnesian elements are highest in the biotite-hornblende gneiss (Fe_2O_3t = 4.65 – 5.44 wt. %, and MgO = 1.79 – 2.07 wt. %), and lowest in the felsic augen gneiss (Fe_2O_3t = 1.11 wt. %, and MgO = 0.12 wt. %). The biotite gneiss, on the other hand, has intermediate content of the ferromagnesian elements (Fe_2O_3t = 2.45 – 4.47 wt. %, and MgO = 0.61 – 0.74 wt. %). The migmatites show lower concentrations of SiO_2 (61.7 – 66.3 wt. %) than the gneisses; nonetheless, they have higher contents of the ferromagnesian elements (Fe_2O_3t = 4.07 – 6.70 wt. %, and MgO = 1.43 – 2.88 wt. %) than the gneisses. The intrusive granitoids have SiO_2 content of 64.7 – 74.0 wt. %, Fe_2O_3 of 1.49 – 3.65 wt. %, and MgO of 0.29 – 1.13 wt. %. The pegmatite also has a SiO_2 content of 71.9 wt. %, Fe_2O_3 of 0.99 wt. % and MgO of 0.22 wt. %. The migmatites and biotite-hornblende gneiss have low K_2O/Na_2O values (K_2O/Na_2O = 0.2 – 0.7 and 0.1 – 0.5, respectively). The biotite gneiss, intrusive granitoids, felsic augen gneiss and pegmatite have high K_2O/Na_2O values (K_2O/Na_2O = 0.5 – 1.3, 0.7 – 1.4, 1.3, and 3.9), respectively.

All the samples plotted in the igneous field on the SiO_2 vs. TiO_2 diagram (Figure 7(a)). The intrusive granitoid, pegmatite and felsic augen gneiss are slightly peraluminous. However, the biotite-hornblende and biotite gneisses show both metaluminous and weak peraluminous signatures (Figure 7(b)). Generally, the rocks have typical I-type signatures (Figure 7(b)). The intrusive granitoids, biotite gneiss, pegmatite and felsic augen gneiss are classified as granite, except one sample each of the intrusive granitoid and biotite gneiss that plot as quartz monzonite (Figure 7(c)). The migmatites show variable compositions as they plot as granodiorite, monzonites and on the boundary line between monzonite and quartz-monzonite (Figure 7(c)). The biotite-hornblende gneiss shows major element compositions akin to granodiorite. On the feldspar normative diagram after O'Connor (1965) (Figure 7(d)), the intrusive granitoids and biotite gneiss dominantly plot as granite, with one sample each plotting as trondjhemite. The pegmatite and felsic augen gneiss are classified as granite, with the biotite-hornblende gneiss plotting entirely as tonalite. The migmatites are classified as granodiorite and tonalite. The felsic augen gneiss, biotite gneiss, migmatite and intrusive granitoids are High-K calc-alkaline in nature (Figure 7(e)). However, one sample of each of the biotite gneiss and migmatite shows Medium-K calc-alkaline and Low-K tholeiite signature, respectively. The biotite-hornblende gneiss has Low-K tholeiite and Medium-K calc-alkaline signatures (Figure 7(e)). The migmatite, biotite-hornblende gneiss and pegmatite are magnesian, whereas the intrusive granitoids and biotite gneiss are both magnesian and ferroan (Figure 7(f)). The felsic augen gneiss plots in the ferroan field (Figure 7(f)).

The granitoids of the internal nappes zone of the Dahomeyide belt show a wide range of trace element concentrations. These wide variations of trace element concentrations have resulted in distinct REE patterns on the chondrite-normalized REE diagram by Palme and O'Neill (2014). The biotite gneiss shows gentle negative slopes with enrichment of the Light Rare Earth Elements (LREE) relative to the Heavy Rare Earth Elements (HREE) and pronounced negative Eu anomalies (Figure 8(a); La/Yb = 12.2 – 32.3; Eu/Eu* = 0.4 – 0.5). The migmatites and biotite-hornblende gneiss depict similar REE patterns characterized by LREE enrichment and nearly flat HREE (Figures 8(b) and (c); La/Yb = 5.5 – 9.3 and 5.3 – 7.4, respectively). However, the migmatites show more noticeable Eu anomalies than the biotite-hornblende gneiss (Figure 8(b); Eu/Eu* = 0.6 and 0.7, respectively). Although the REE pattern for the felsic augen gneiss resembles that of the migmatites, the HREEs are slightly depleted in the felsic augen gneiss with pronounced Eu anomalies compared to the migmatites (Figure 8(d); La/Yb = 9.2; Eu/Eu* = 0.4). The intrusive granitoids show a steep negative slope depicted by enrichment of the LREE and a significant depletion of the HREE and pronounced negative Eu anomalies (Figure 8(e); La/Yb = 40.9 – 47.4; Eu/Eu* = 0.3 – 0.6). Conversely, the pegmatite shows LREE enrichment, HREE depletion and positive Eu anomaly (Figure 8(f); La/Yb = 34.9; Eu/Eu* = 1.0). On the incompatible multi-element normalized to primitive mantle diagrams, the biotite gneiss is enriched in the LILE relative to the HFS with negative peaks in Ba, Nb-Ta, Sr P and Ti (Figure 9(a)). The patterns depicted by the migmatites and biotite-hornblende gneiss are characterized by both LILE enrichment and depletion and nearly flat HFS, with negative peaks in Nb-Ta, P and Ti (Figures 9(b) and (c)). Their overall trace element concentration is lower than the biotite gneiss. The felsic augen gneiss shows an incompatible trace elements pattern comparable to the biotite gneiss (Figure 9(d)) except for the positive peak in K. The intrusive granitoids show enrichment of the LILE and a significant depletion of the HFS and pronounced negative Nb-Ta, P and Ti peaks (Figure 9(e)). The pegmatite, on the other hand, shows LILE enrichment, HFS depletion, positive K and Sr peaks and negative Nb-Ta, P and Ti peaks (Figure 9(f)).

7. Discussion

7.1. Significance of the deformational events to the Pan-African orogeny

From a broader perspective, our detailed structural analysis suggests that the internal nappes zone of the Dahomeyide belt, southeastern Ghana, has been affected by a major NW-SE shortening followed by NW-SE thrusting and a later extension

https://doi.org/10.1017/S0016756823000808 Published online by Cambridge University Press

Table 2. Major and trace element data of internal nappes zone of the Dahomeyide belt

Felsic Augen gneiss		Biotite gneiss				Migmatite		
SAMPLE	ENK03	EN09	ENAQ6	ENMTS01	ENK01	ENAQ8	ENAQ1	ENMTS02
wt. %								
SiO_2	76.2	70.8	70.6	70.8	69.1	61.7	62.9	66.3
TiO_2	0.08	0.43	0.31	0.45	0.52	0.71	0.73	0.55
Al_2O_3	14.25	14.25	15.25	14.65	14.8	16.1	16.65	14
Fe_2O_3	1.11	2.99	2.45	3.05	4.47	6.59	6.7	4.07
MnO	0.04	0.05	0.05	0.05	0.06	0.1	0.1	0.14
MgO	0.12	0.61	0.74	0.66	0.66	2.85	2.88	1.43
CaO	1.3	1.84	2.69	2.05	2.24	2.74	2.82	6.12
Na_2O	3.7	3.5	4.66	3.76	3.96	4.1	4.21	4.38
K_2O	4.81	4.48	2.45	4.24	4.23	2.95	3.06	0.67
P_2O_5	0.02	0.11	0.15	0.12	0.14	0.17	0.18	0.13
LOI	0.3	0.26	0.6	0.4	0.62	0.69	0.67	0.33
Total	102	99.41	100.05	100.32	100.9	98.79	100.99	98.16
Mg#	18	29	37	30	23	46	46	41
ppm								
Co	1	5	5	5	6	18	17	9
Ni	2	4	6	4	4	33	32	14
Cr	10	10	20	10	10	60	60	30
V	5	23	35	23	25	123	125	86
Sc	2	7	4	6	7	17	17	11
Ga	19	20.3	21.6	20.5	25.3	17.8	18.7	14.7
Pb	20	19	16	21	14	11	9	11
Cs	0.72	6.91	3.05	6.55	1.72	14	13	1.45
Rb	105.5	196	111	186.5	115.5	179	182	42.2
Ba	459	627	642	624	771	453	451	94.9
Th	11.5	25.6	16.05	21.7	17.15	5.27	5.5	4.8
U	2.2	7.1	2.97	2.78	1.56	1.81	2.02	3.25
Nb	11.4	25.6	15	28.6	36.8	8.6	9.7	10.7
Ta	0.2	2.5	1	2.8	1.9	0.5	0.6	1.7
La	15.5	71.2	41.1	52.2	66	23.8	23.5	19.2
Ce	30	142.5	86.1	105	133.5	46.8	46	38.2
Pr	3.44	15.65	9.46	11.8	15.2	5.61	5.55	4.7
Sr	156	168	271	181	190	298	293	280
Nd	12.7	56.7	35.5	43.3	57.8	22.8	21.8	19.3
Sm	3.18	9.82	6.49	8.64	11.8	4.98	4.57	4.46
Zr	84	265	253	276	372	157	172	145
Hf	3.6	7.8	6.7	7.9	10.2	4.3	4.7	4
Eu	0.65	0.94	0.96	0.9	1.17	1.01	1.11	1.06
Gd	2.7	7.48	4.32	6.89	10.6	4.2	3.97	4.26
Tb	0.42	1.06	0.57	1.03	1.67	0.63	0.64	0.7
Dy	2.45	5.76	2.82	5.8	9.62	3.78	3.66	4
Y	13.6	28.7	13.4	28.8	49.1	19.6	18.3	24

(*Continued*)

https://doi.org/10.1017/S0016756823000808 Published online by Cambridge University Press

Table 2. (*Continued*)

Felsic Augen gneiss		Biotite gneiss				Migmatite		
SAMPLE	ENK03	EN09	ENAQ6	ENMTS01	ENK01	ENAQ8	ENAQ1	ENMTS02
Ho	0.47	0.99	0.52	1.04	1.93	0.78	0.73	0.83
Er	1.39	2.72	1.16	2.84	5.23	2.24	2.03	2.38
Tm	0.21	0.36	0.15	0.39	0.68	0.34	0.28	0.34
Yb	1.18	2.33	0.89	2.24	3.79	2.22	1.76	2.46
Lu	0.17	0.32	0.13	0.36	0.57	0.31	0.28	0.36

	Hornblende-biotite gneiss			Pegmatite	Intrusive granitoids				
SAMPLE	ENAQ3	ENAQ9	ENAQ90	ENAQ02	ENK02	EN12	ENKP03	EN13	ENAQ4
wt. %									
SiO_2	66.5	63.6	64.5	71.9	64.7	74	74	72.2	70.9
TiO_2	0.64	0.64	0.59	0.12	0.75	0.18	0.19	0.21	0.37
Al_2O_3	14.8	13.4	13.75	14.7	15.95	14.15	14.55	14.33	14.88
Fe_2O_3	5.11	5.44	4.65	0.99	3.65	1.51	1.49	3.33	2.22
MnO	0.11	0.2	0.18	0.01	0.03	0.03	0.03	0.03	0.03
MgO	2.07	1.79	1.67	0.22	1.13	0.29	0.33	0.44	0.58
CaO	3.1	9.5	8.34	0.66	2.67	1.46	1.59	1.86	1.91
Na_2O	3.95	4.04	4.28	2.17	4.73	3.68	3.75	3.08	4.05
K_2O	2.16	0.3	0.31	8.55	3.31	4.41	4.6	4.16	4.11
P_2O_5	0.16	0.18	0.14	0.02	0.25	0.05	0.06	0.18	0.12
LOI	0.66	0.35	0.31	0.43	1.01	0.24	0.67	0.96	0.64
Total	99.39	99.5	98.78	100.06	98.39	100.1	101.39	100.80	99.96
Mg#	45	39	42	31	38	28	30	21	34
ppm									
Co	12	12	10	2	8	2	1	6	4
Ni	15	19	16	2	5	2	2	5	3
Cr	40	50	90	10	10	10	10	15	10
V	117	122	107	6	75	7	10	46	31
Sc	14	13	11	1	3	2	2	4	2
Ga	14.8	14.5	14.7	12.8	20.9	18.7	17.6	28.60	19.07
Pb	9	12	14	36	10	25	31	33	22
Cs	6.49	0.13	0.1	3.22	1.27	5.77	2.85	4.95	3.30
Rb	100.5	3.9	3.6	232	107	186.5	162	228	152
Ba	633	76.6	73.7	2330	1365	720	880	1483	988
Th	3.07	3.75	3.89	4.27	10.05	21.4	11.55	21.5	14.33
U	1.02	2.09	2.68	2.35	0.63	1.86	1.53	2.01	1.34
Nb	6.3	6.3	7.9	4	10.2	14.2	9.6	17.0	11.3
Ta	0.7	0.5	0.9	0.5	0.7	0.7	0.5	1.0	0.6
La	15.8	19.6	19	14	75.9	36.2	23.4	67.8	45.2
Ce	33.5	37	39.2	21.8	148.5	69.8	42.9	130.6	87.1
Pr	4.27	4.31	4.8	2.19	15.95	7.49	4.55	14.00	9.33
Sr	443	345	352	330	527	182.5	274	492	328
Nd	18.1	17.7	19.6	7.8	56.7	26.7	16.5	50.0	33.3
Sm	3.69	3.62	4.23	1.42	8.37	5.07	3.11	8.28	5.52

(*Continued*)

https://doi.org/10.1017/S0016756823000808 Published online by Cambridge University Press

Table 2. (*Continued*)

	Hornblende-biotite gneiss			Pegmatite	Intrusive granitoids				
SAMPLE	ENAQ3	ENAQ9	ENAQ90	ENAQ02	ENK02	EN12	ENKP03	EN13	ENAQ4
Zr	126	148	147	31	377	132	107	308.00	205.33
Hf	3.5	3.9	4.1	1	8	4.3	3.4	7.9	5.2
Eu	1.09	1.12	1.24	0.96	1.51	0.55	0.58	1.32	0.88
Gd	3.63	3.69	4.04	0.97	4.89	3.7	2.37	5.48	3.65
Tb	0.55	0.56	0.6	0.1	0.58	0.47	0.31	0.68	0.45
Dy	3.44	3.24	3.72	0.46	2.75	2.17	1.25	3.09	2.06
Y	20.6	19.4	23.1	2.5	13.5	10.2	5.8	14.75	9.83
Ho	0.75	0.66	0.79	0.08	0.47	0.36	0.21	0.52	0.35
Er	2.28	2.16	2.47	0.2	1.26	0.78	0.53	1.29	0.86
Tm	0.35	0.31	0.36	0.04	0.18	0.11	0.05	0.17	0.11
Yb	2.26	1.85	2.49	0.28	1.12	0.55	0.4	1.04	0.69
Lu	0.32	0.31	0.4	0.04	0.13	0.09	0.04	0.13	0.09

event (orogenic collapse). These shortening, thrusting and extension events are expressed as four deformation phases (D_1-D_4), which occurred during various stages of the Pan-African orogeny. The D_1 phase is widespread and represents NW-SE Pan-African shortening associated with the regional phase of crustal movement that resulted in westward nappe piling during the Pan-African continent-continent collision between the West African Craton (WAC) and BNS. Attoh et al. (2007) and Kwayisi et al. (2020) have suggested that the transition from continental subduction to continent-continent collision resulted in a change in orogenic structural grain from N-S to NE-SW fabric. Rotation of regional E-W shortening direction to NW-SE shortening direction produced the NE-SW fabrics between 600 and 580 Ma. The presence of asymmetric quartz porphyroblasts indicates a shearing component with a general dextral top-to-the-NE sense of movement during the D_1 event.

The D_2 deformational regime followed the D_1 shortening shear deformation, representing a Pan-African thrusting event as a result of progressive NW-SE shortening. Thrusting resulted in the transposition of the D_1 fabrics. The D_2 deformation is a ductile shear deformation that formed S_2 foliations (cleavages), F_2 folds, kink folds and coeval with C_2 shear faults. The main kinematic indicators associated with the D_2 event are the near horizontal NW-dipping L_2 stretching lineation and small-scale C_2 shear faults with a top-to-the-NW dextral sense of movement observed in the field and processed aeromagnetic data (Figures 5(c), (d) and 6(d)). D_2 corresponds probably with west-verging thrusting and exhumation of the HP rocks between 590 and 580 Ma (Attoh et al. 1997; Affaton et al. 2000). The main S_1 foliations are observable in microscopic and mesoscopic scales and are much more spectacular than the younger S_2 foliations. This means the D_1 event was rather intense, with better-preserved structures than the D_2 event. This interpretation is backed by shallow inter-limb angle and parallel limbed isoclinal folds associated with the D_1 tectonic phase.

The D_3 event corresponds to a shear deformational regime in which the sinistral shear faults were produced. The D_4 brittle tectonic event marked the last deformational and geological event in the evolutionary sequence of the internal nappes zone of the Dahomeyide belt. The significance of the D_3 and D_4 deformational events is unclear; however, D_3 could be a continuation of the thrusting phase of the Pan-African orogeny since it shares similar structural grains as D_2, whereas D_4 may be linked to the extensional-related volcanic and sedimentary rocks formed after Pan-African continent-continent collision (Ganade de Araujo et al. 2016).

7.2. Tectonic setting

Petrographical investigation revealed that the rocks had undergone very minimal alteration and that, coupled with the very low Loss on Ignition (LOI) values (<1.05 wt. %), suggests insignificant elemental mobility; thus, the major and trace element compositions can be utilized in tectonic setting and petrogenetic interpretations. The internal nappes zone has been proposed to be a juvenile arc crust with pockets of reworked Paleoproterozoic rocks intruded by post-collisional granitoids, representing the active margin of the Dahomeyide belt (Kalsbeek et al. 2012; Attoh et al. 2013). Field, petrographical and structural data reveal two main rock categories. These are (i) deformed rocks made up of gneisses and migmatites and (ii) undeformed rocks comprising mainly intrusive granitoids of granite and granodiorite composition (Figures 2, 3, and 4). Several tectonic discrimination diagrams, coupled with trace element patterns and ratios, have been used to assess the tectonic setting of the formation of these granitoids. The overall trace element patterns of the studied granitoids are characterized by enrichment of LILE and depleted HFS, with negative peaks of Nb-Ta, Sr, P and Ti (Figure 9). These geochemical features are typically considered as indications of subduction processes (Spandler and Pirard, 2013; Kelemen et al. 2014). Except for three samples of biotite gneiss that plot in the within-plate granitoid field, all the other samples plot in the field defined by volcanic-arc and syn-collisional granitoids (Figure 10(a)). The Zr verses $(Nb/Zr)_N$ diagram by Thiéblemont and Tégyey (1994) suggests the pegmatite, felsic augen gneiss, biotite gneiss and majority of the intrusive granitoids show geochemical signatures typical of granitoids derived from continent-continent collision, i.e. active margin environment (Figure 10(b)). The biotite-hornblende gneiss, migmatites and two samples of biotite gneiss plot within the arc-array and the field defined by continental arc (Figure 10(c)).

https://doi.org/10.1017/S0016756823000808 Published online by Cambridge University Press

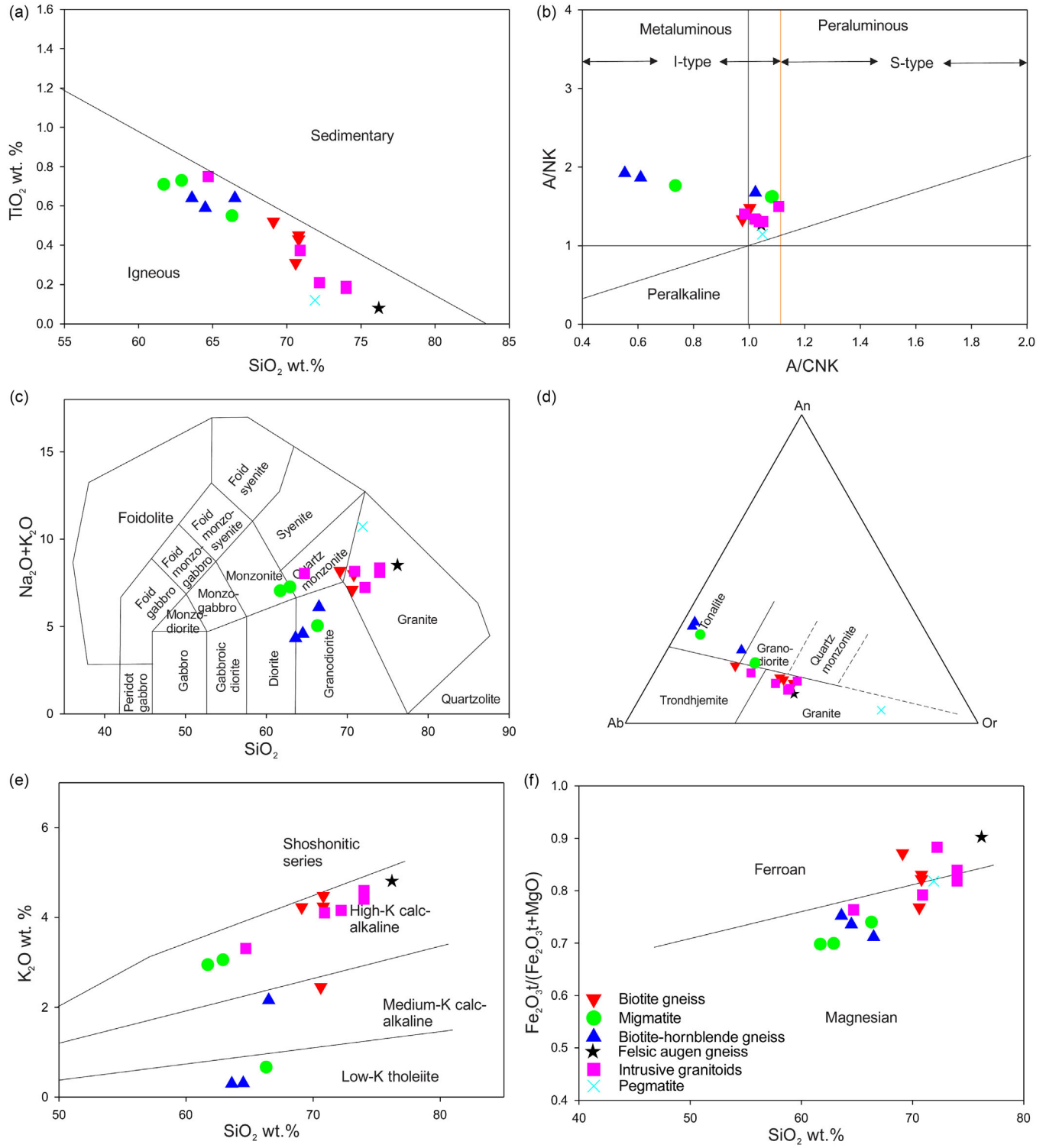

Figure 7. (Colour online) Major element classification diagrams of the gneisses, migmatite and intrusive granitoids of the internal nappes zone (a) Plot of SiO_2 vs. TiO_2 (Tarney 1977), (b) Plot of A/CNK (molar $Al_2O_3/(CaO + Na_2O + K_2O)$) vs. ANK (molar $Al_2O_3/(Na_2O + K_2O)$) (Maniar and Piccoli 1989), (c) Total alkalis vs silica (Middlemost 1985), (d) Or-Ab-An ternary diagram (O'Connor, 1965), (e) K_2O vs. SiO_2 diagram (after Peccerillo and Taylor 1976) and (f) SiO_2 vs. $FeO_t/(FeO_t+MgO)$ diagram (after Frost and Frost 2008).

Although the felsic angen gneiss, pegmatite, biotite gneiss and intrusive granitoids plot in the continental arc field, they plot slightly away from the arc-array field (Figure 10(c)). This geochemical feature may suggest significant crustal contamination of the intrusive granitoids and pegmatite, and to some extent, the biotite and felsic augen gneisses.

R1 (4Si-11(Na+K)-2(Fe+Ti)) verse R2 (6Ca+2Mg+Al) tectonic discriminating diagram (after Batchelor and Bowden, 1985) (Figure 10(d)) puts the rocks of the internal nappes zone into various orogenic phases consistent with field and petrographical evidence. On this diagram, the biotite-hornblende gneiss shows pre-collisional signatures. At the same time, the migmatites

https://doi.org/10.1017/S0016756823000808 Published online by Cambridge University Press

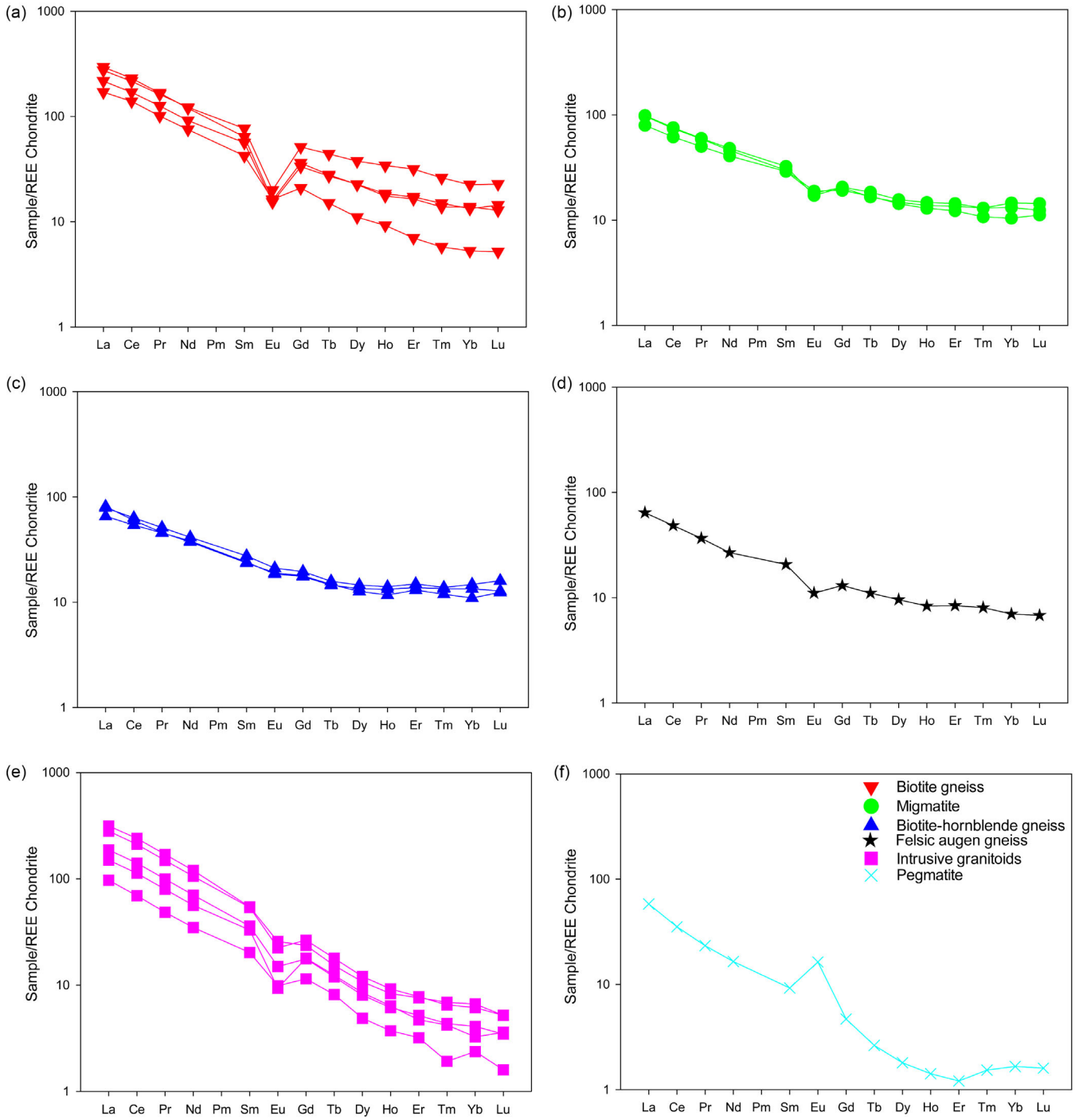

Figure 8. (Colour online) Chondrite-normalized REE diagrams of (a) biotite gneiss, (b) Migmatites, (c) biotite-hornblende gneiss, (d) felsic augen gneiss, (e) intrusive granitoids and (f) pegmatite. Chondrite and primitive normalizing values are from Palme and O'Neill, (2014).

straddle between pre and syn-collisional settings, with the biotite and felsic augen gneisses showing syn-collisional features. The intrusive granitoids plot in the late orogenic field, with the pegmatite plotting between syn-collision and an orogenic granite boundary (Figure 10(d)). Typical collisional features such as foliations and folds, which occur in most of the gneisses and migmatites, represent the compressive stages of orogenesis. The deformed rocks (gneisses and migmatites) of the internal nappes zone with dominant axial planar foliations indicate their formation in a collisional setting or were affected by the Pan-African collisional process. The continental-arc signatures imply continental subduction processes in their formation. The intrusive granitoids and pegmatite are undeformed, implying late- to post-orogenic emplacement; thus, the continental-arc features could result from contamination during their evolution.

https://doi.org/10.1017/S0016756823000808 Published online by Cambridge University Press

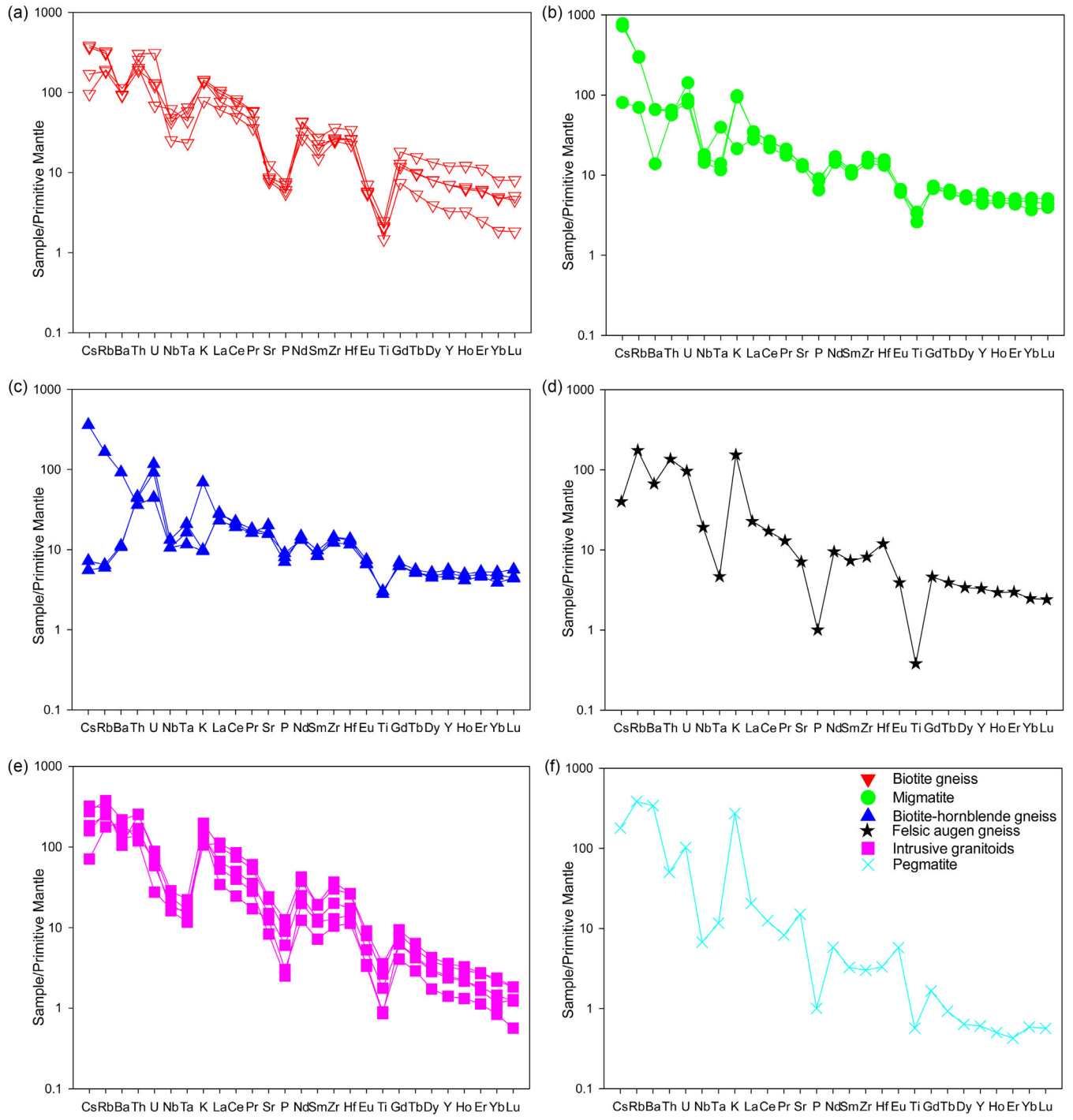

Figure 9. (Colour online) Primitive mantle-normalized diagrams of (a) biotite gneiss, (b) Migmatites, (c) biotite-hornblende gneiss, (d) felsic augen gneiss, (e) intrusive granitoids and (f) pegmatite. Chondrite and primitive normalizing values are from Palme and O'Neill (2014).

7.3. Petrogenesis

7.3.1. Lithological evolution

Petrographical and geochemical studies indicate that the rocks of the internal nappes zone are gneisses, migmatite and intrusive granitoids of granite, granodiorite and tonalite with minor trondjhemite compositions, formed during and after the Pan-African subduction-collision events. The gneisses and migmatites are pre- to syn-collisional granitoids, whereas the intrusive granitoids are post-collisional. Results of this study show that the migmatites are the most abundant rock in the Pan-African Dahomeyide internal nappes zone in southeastern Ghana, suggesting widespread migmatization during the Pan-African orogeny. The migmatites consist of biotite-rich gneissic melanosomes and feldspar-rich granitic leucosomes, resulting in lithological heterogeneity. Johnson et al. (2013) suggested that granitic leucosomes with abundant K-feldspar represent areas dominated by segregated crystal melt. Sawyer (1999) also described melanosomes as evident sites of melt formation, while leucosomes

https://doi.org/10.1017/S0016756823000808 Published online by Cambridge University Press

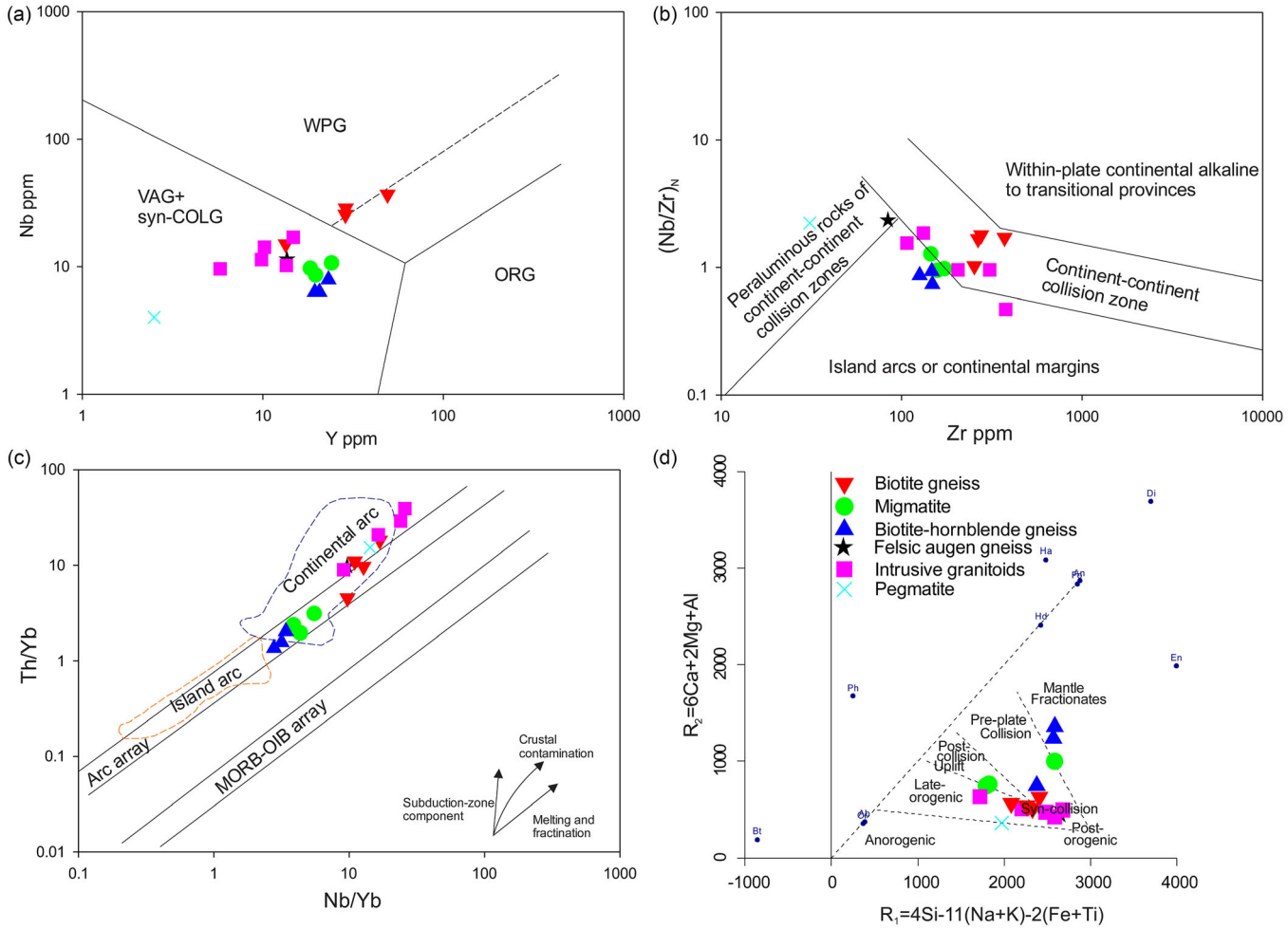

Figure 10. (Colour online) Tectonic discriminant diagrams for the rocks of the internal nappes zone of the Dahomeyide belt (a) Nb vs. Y after Pearce et al. (1984), (b) Zr vs. (Nb/Zr)N diagram of Thiéblemont and Tégyey (1994), (c) Th/Yb vs. Nb/Yb with reference fields modified after Pearce (2008) and (d) R1-R2 (after Batchelor and Bowden, 1985).

are sites of melt collection. From field and petrographical data, these features are characteristics of the migmatites of the Dahomeyide internal nappes zone, which suggests the migmatites resulted from partial melting of pre-existing rocks (gneisses) following Kornprobst (2002). Consequently, the lithological heterogeneity observed in the migmatites may be due to partial melting of the gneisses. Geochemical classification diagrams indicate that the migmatites and biotite-hornblende gneiss evolved from similar granodioritic-tonalitic protolith (Figures 7(c) and (d)). Thus, the migmatites might have evolved from the biotite-hornblende gneiss through crustal anataxis during amphibolite facies metamorphism (Table 1), as described by Nude (1995).

Field relations, including cross-cutting relationships, gradational and sharp lithological contact, and inclusions, among others, have been used to establish the relative formation period of the gneisses, migmatite and intrusive granitoids of the internal nappes zone. The leucosomes slightly cut across the melanosomes in the migmatites, implying that the former is relatively younger than the latter. Textural evidence shows that the melanosome is rich in biotite but more depleted in feldspars and quartz than the leucosome. The felsic augen gneiss may have formed due to the gradual mineral growth associated with metamorphism and shearing. Gradational boundaries between the migmatites and gneisses imply a gradual transition from gneiss to migmatite with increasing temperature and the onset of partial melting. Pockets of gneisses occur within the intrusive granitoids, and this, coupled with the sharp contacts between the intrusive granitoids and gneisses (Figures 4(a) and (b)), indicate an intrusive relationship between the two. Besides, the gneisses are significantly deformed, whereas the intrusive granitoids are undeformed. The intrusive granitoids, biotite gneiss and felsic augen gneiss share similar lithological compositions, i.e., granite and granodiorite (Figure 7(c) and (d)). This may be a manifestation of the derivation of the intrusive granitoids from the partial melting of the biotite and felsic augen gneisses. This could explain the similar REE, LILE and HFS patterns depicted by the intrusive granitoids and the biotite gneiss on the REE and multi-element diagrams (Figures 8 and 9). In addition, these rocks show similar tectonic setting characteristics (Figure 11). The cross-cutting relationship between the pegmatite veins and migmatitic layers indicates a relatively younger age of the pegmatite than the migmatites.

7.3.2. Magma source and depth of emplacement

Major and trace elements geochemical data in Table 2 show low Mg (Mg# = 14.77-44.5), very low Ni (1-19ppm) and Cr (10-50ppm) contents for the gneisses, migmatite and intrusive granitoids. These features suggest the formation of the gneisses, migmatite and intrusive granitoids from evolved magmas rather

https://doi.org/10.1017/S0016756823000808 Published online by Cambridge University Press

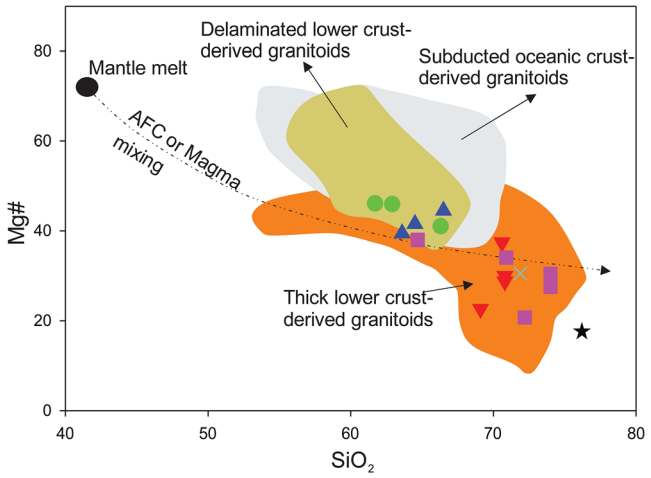

Figure 11. (Colour online) SiO_2 vs. Mg# plot for the rocks of the internal nappes zone of the Dahomeyide belt for petrogenetic interpretation. Fields of mantle, subducted oceanic crust, pure oceanic crust, delaminated lower crust, thick lower crust and metabasalt and eclogite melts are from Wang et al. (2006).

than primary magmas whose Mg# >65, Cr >1000 ppm, and Ni >400-500 ppm (Winter, 2001). The rocks of the internal nappes zone of the Dahomeyide belt, southeastern Ghana, are generally I-type granitoids with metaluminous and weak peraluminous features (Figure 7(b)). The intrusive granitoids, biotite and felsic gneisses and some of the migmatite are High-K calc-alkaline in nature. Partial melting of crustal rocks, or subduction-influenced mantle, has been proposed to generate High-K calc-alkaline granitoids (Gläser et al. 2022). The High-K calc-alkaline signature and their I-type nature may suggest the melting of older igneous crustal materials. Besides, the intrusive granitoids show similar lithological compositions and trace element characteristics as the biotite gneiss, indicating partial melting of the latter to form the former. The Low-K tholeiite, metaluminous and I-type signatures of the biotite-hornblende gneiss and one sample of the migmatites suggest the melting of intermediate to mafic rocks. All the rocks of the internal nappes zone have Mg# values akin to granitoids derived from the lower crust (Figure 11).

The gneisses, migmatite and intrusive granitoids show LREE enrichment relative to HREE with a pronounced Eu negative (Eu/Eu*) anomaly, except for the pegmatite, which has a positive Eu anomaly. The REE pattern, together with the negative Ba, Sr and Eu anomalies, might be associated with residual plagioclase at the source or formation of their magmas in an oxidized environment, such as the continental crust (Rudnick and Gao, 2014). The continental crust is typically enriched in LREE and LILE but strongly depleted in Ti, Nb and Ta (Rollinson (1993), as is the case of the gneisses, migmatite and intrusive granitoids of the internal nappes zone (Figures 8 and 9). The depletion in Ti, Nb and Ta, evident on the primitive mantle normalized multi-element plot (Figure 9), together with weak positive Zr-Hf anomalies exhibited by the rocks, are diagnostic characteristics of the continental crust, while the depletion in Ba suggests an active margin source (Elburg, 2010; Rudnick and Gao, 2014). Negative Nb-Ta and Ti anomalies suggest relative enrichment of other elements by fluids or melt from a subducting plate in an arc setting (Elburg, 2010). The low Sr/Y ratios, with corresponding high Yb >1.5 ppm and Y >10 ppm content for the rocks of the internal nappes zone, support the melting of crustal material in their formation. On the SiO_2 verse Mg# (Figure 11), the migmatites and biotite-hornblende gneiss plot in the region of delaminated lower crust-derived granitoids, whereas the biotite and felsic augen gneisses, intrusive granitoids and pegmatite plot in the field of thick lower crust-derived granitoids. This suggests the melting of a delaminated and/or thickened lower crust to form the gneisses, migmatite and intrusive granitoids.

Field studies have revealed that the gneisses and migmatites are deformed, with deformation features defined by foliations, folds, thrust and shear zone. These deformational features have been attributed to major shortening, shearing and thrusting events during the Pan-African orogeny. Such structures provide a historical record of deep (middle to lower) crustal level emplacement and deformation of the rocks (Opare-Addo et al. 1993). Thus, it is likely that the depth of emplacement of these rocks is $\leq$ 35 km (lower crust) (Hacker et al. 2015; Aidoo et al. 2020; Aidoo et al. 2021). This is confirmed by the SiO_2 verse Mg# diagram (Figure 11), where the granitoids show geochemical characteristics of delaminated and/or thick lower crust.

7.4. Implications for crustal growth and evolution of the Dahomeyide belt active margin

Petrographical investigation and geochemical signatures suggest that the gneisses, migmatite and intrusive granitoids of the internal nappes zone, which represents the active margin of the Dahomeyide belt, are I-type, metaluminous and weakly peraluminous granitoids of tonalite, granodiorite and granite signatures formed during pre-, syn- and post-collisional orogenic setting. In this study, the biotite-hornblende gneiss formed during the pre-orogenic phase of the Pan-African orogeny in an arc setting. This gneiss may correspond to the basement of the Benin-Nigerian shield (Duclaux et al. 2006; Attoh et al. 2013). Older U-Pb zircon crystallization ages ranging from 2.14 to 2.19 Ga recorded for the hornblende gneiss have been interpreted to suggest the involvement of older Paleoproterozoic crust (Saharan Metacraton), representing the basement of the Benin-Nigerian Shield, in the Pan-African Dahomeyide belt (Duclaux et al. 2006; Attoh et al. 2013). The biotite-hornblende gneiss in this study shows tonalite and granodiorite composition. Hence, the Paleoproterozoic basement of the Benin-Nigerian Shield evolved from I-type, metaluminous, tonalitic-granodioritic magma emplaced in a continental-arc setting. This was later deformed and remobilized (migmatized) during the Pan-African orogeny.

Tectonic discriminations suggest continental arc and continent-continent collision for the migmatites and biotite gneiss, respectively (Figure 10). Plate convergence (both ocean and continental subduction) and arc magmatism formed approximately 670 to 630 Ma, followed by continent-continent collision of the WAC with the BNS between 620 and 610 Ma, which is characterized by HP metamorphism have been proposed as the geodynamic evolution of the Dahomeyide belt (Attoh, 1998; Agbossoumondé et al. 2001; Duclaux et al. 2006; Attoh and Nude, 2008; Ganade de Araujo et al. 2016). A double subduction system (island arc and active continental margin) occurred in the north (Benin and northern Togo), which evolved into a single subduction system (continental subduction) in the south (Ghana; Guillot et al. 2019). This was followed by a continent-continent collision between the WAC and the Benin-Nigerian Shield (Kwayisi et al. 2020). Thus, the migmatites might have formed during the continental subduction phase of the Pan-African orogeny and later metamorphosed and deformed during the continent-continent collision between the WAC and BNS. This occurred due to the partial melting of the continental crust (i.e. the biotite-hornblende gneiss) of tonalite and

https://doi.org/10.1017/S0016756823000808 Published online by Cambridge University Press

granodiorite affinity at a depth of ≤35 km (Figure 11). This implies that large-scale migmatization occurred during the convergence process of the Pan-African orogeny through crustal anatexis.

Geochemical features of the intrusive granitoids and some of the biotite gneiss indicate High-K calc-alkaline granitoids formed by partially melting the thick lower crust in a post-collisional setting. According to Liégeois et al. (1998), a post-collisional environment characterized by substantial motions along shear zones could have resulted in the re-melting of an earlier continental crust due to subduction in the lithospheric mantle or lower crust. Furthermore, Lu et al. (2015) and Eglinger et al. (2017) revealed that High-K calc-alkaline and shoshonitic granitoids are frequently placed in arc and post-collisional settings, preceded by a crustal thickening phase. The Dahomeyide belt post-collisional magmatism occurred between 580 and 540 Ma (Kalsbeek et al. 2012; Attoh et al. 2013; Ganade de Araujo et al. 2016; Guillot et al. 2019). Thus, the active margin of the Dahomeyide belt evolved during the subduction-collisional and post-collisional phases of the Pan-African orogeny between the Cryogenian and Ediacaran periods (670 – 540 Ma). This evolution witnessed large-scale migmatisation, crustal thickening and granitoid intrusions through partial melting of the thickened continental crust. The growth of the active margin occurred through tonalite-granodiorite magmatism due to the partial melting of the delaminated lower crust. This was followed by large-scale migmatization due to the remobilization of pre-existing crustal rocks during continental subduction. Then, crustal thickening due to continent-continent collision followed by melting of the thickened crust to form the intrusive granitoids (granite and granodiorite).

8. Conclusion

Integrated field, petrographical, geophysical, structural and geochemical studies of granitoids from the internal nappes zone (i.e., active margin) of the Dahomeyide belt are presented in this research. Two main lithological units, (i) deformed meta-granitoids made up of migmatites and gneisses and (ii) undeformed granitoids, including granite and granodiorite, dominate the internal nappes zone of southeastern Ghana. These granitoids have been affected by four deformation phases (D_1-D_4) during a major NW-SE shortening followed by NW-SE dextral-sinistral thrusting and a later extensional event during the Pan-African orogeny. Petrographical and geochemical studies indicate that the gneisses, migmatite and intrusive granitoids of the internal nappes zone are of granite, granodiorite and tonalite composition, formed during and after the Pan-African subduction-collision events. The gneisses and migmatite with dominant foliations and folds indicate their formation in a collisional setting or were affected by the Pan-African collisional process because these features are associated with compressive processes. The continental-arc signatures of the gneisses and migmatites imply continental subduction processes in the formation of their protolith. The intrusive granitoids are undeformed, implying late- to post-orogenic emplacement; thus, the continental-arc features could result from contamination during their evolution. The active margin of the Dahomeyide belt evolved during the subduction-collisional and post-collisional phases of the Pan-African orogeny. This evolution witnessed large-scale migmatization and granitoid intrusions through partial melting of thickened continent crust.

Acknowledgement. The authors thank the Department of Earth Science Capacity Building Project for supporting this research financially.

References

Abdelsalam MG, Liégeois J-P and Stern RJ (2002) The Saharan metacraton. *Journal of African Earth Sciences* **34**(3–4), 119–136.

Affaton P, Kröner A and Seddoh KF (2000) Pan-African granulite formation in the Kabye Massif of Northern Togo (West Africa): Pb–Pb zircon ages. *International Journal of Earth Sciences* **88**, 778–790.

Affaton P, Rahaman MA, Trompette R and Sougy J (1991) The Dahomeyide Orogen: Tectonothermal evolution and relationships with the Volta Basin. In The *West African Orogens and Circum-Atlantic Correlatives* (eds RD Dallmeyer and JP Lécorché), pp. 107–122. Berlin; Heidelberg: Springer.

Agbossoumondé Y, Ménot R-P and de Araujo CG (2017) Major, trace elements and Sr-Nd isotopic characteristics of high-pressure and associated metabasites from the Pan-African Suture Zone of Southern Togo. West Africa. *Journal of Environmental and Earth Science* **7**, 17–31.

Agbossoumondé Y, Ménot R-P and Guillot S (2001) Metamorphic evolution of Neoproterozoic eclogites from south Togo (West Africa): geodynamic implications for the reconstruction of west Gondwana. *Journal of African Earth Sciences* **33**(2), 227–244.

Agyei-Duodu J, Loh GK, Boamah KO, Baba M, Hirdes W, Toloczyki M and Davis DW (2009) Geological map of Ghana **1**:1000 000. Geological Survey Department of Ghana (GSD).

Aidoo F, Nude PM, Sun F-Y, Liang T and Zhang S-B (2021) Paleoproterozoic TTG-like metagranites from the Dahomeyide belt, Ghana: constraints on the evolution of the Birimian-Eburnean orogeny. *Precambrian Research* **353**, 106024.

Aidoo F, Sun F-Y, Liang T and Nude PM (2020) New insight into the Dahomeyide Belt of southeastern Ghana, West Africa: Evidence of arc-continental collision and Neoarchaean crustal reworking. *Precambrian Research* **347**, 105836.

Attoh K (1998) High-pressure granulite facies metamorphism in the Pan-African Dahomeyide orogen, West Africa. *Journal of Geology* **106**, 236–246.

Attoh K, Corfu F and Nude PM (2007) U-Pb Zircon age of deformed carbonatite and alkaline rocks in the Pan-African Dahomeyide suture zone, West Africa. *Precambrian Research* **155**, 251–260.

Attoh K, Dallmeyer RD and Affaton P (1997) Chronology of nappe assembly in the Pan-African Dahomeyide orogen, West Africa: evidence from 40Ar/39Ar mineral ages. *Precambrian Research* **18**, 153–171.

Attoh K and Morgan J (2004) Geochemistry of high-pressure granulites from the Pan-African Dahomeyide orogen, West Africa: constraints on the origin and composition of the lower crust. *Journal of African Earth Sciences* **39**, 201–208.

Attoh K and Nude PM (2008) Tectonic significance of carbonatite and ultrahigh-pressure rocks in the Pan-African Dahomeyide suture zone, southeastern Ghana. *Geological Society, London, Special Publications* **297**, 217–231.

Attoh K, Samson S, Agbossoumondé Y, Nude PM and Morgan J (2013) Geochemical characteristics and U–Pb zircon LA-ICPMS ages of granitoids from the Pan-AfricanDahomeyide orogen, West Africa. *Journal of African Earth Sciences* **79**(2013) 1–9.

Batchelor B and Bowden P (1985) Petrogenetic interpretation of granitoid rock series using multinational parameters. *Chemical Geology* **48**, 43–55.

Chala D, Tairou MS, Wenmenga U, Kwékam M, Affaton P, Kalsbeek F, Tossa C and Houéto A (2015) Pan-African deformation markers in the migmatitic complexes of Parakou–Nikki (Northeast Benin). *Journal of African Earth Sciences* **111**, 387–398.

Duclaux G, Ménot R-P, Guillot S, Agbossoumondé Y and Hilairet N (2006) The mafic layered complex of the Kabyé massif (north Togo and north Bénin): Evidence of a Pan-African granulitic continental arc root. *Precambrian Research* **151**(1–2), 101–118.

Dzikunoo EA, Kazapoe RW and Agbetsoamedo JE (2021) An integrated structural and geophysical approach to defining the structures of part of the Nangodi greenstone belt, northeastern Ghana. *Journal of African Earth Sciences* **180**, 104238.

Eglinger A, Thebaud N, Zeh A, Davis J, Miller J, Parra-Avila LA, Loucks R, McCuaig C and Belousova E (2017) New insights into crustal growth of the Paleoproterozoic margin of the Archaean Kemena-Man domain, West

https://doi.org/10.1017/S0016756823000808 Published online by Cambridge University Press

African craton (Guinea): Implications of gold mineral system. *Precambrian Research* **292**, 258–289.

Elburg MA (2010) Sources and processes in arc magmatism: The crucial role of water. *Geologica Belgica* **13**(3), 121–136.

Frost BR and Frost CD (2008) A geochemical classification for feldspathic igneous rocks. *Journal of Petrology* **49**(11), 1955–1969.

Ganade de Araujo CE, Cordani UG, Agbossoumounde Y, Caby R, Basei MA, Weinberg RF and Sato K (2016) Tightening-up NE Brazil and NW Africa connections: New U–Pb/Lu-Hf zircon data of a complete plate tectonic cycle in the Dahomey belt of the West Gondwana Orogen in Togo and Bénin. *Precambrian Research* **276**, 24–42.

Gläser L, Grosche A, Voudouris PC and Haase KM (2022) The high-K calc-alkaline to shoshonitic volcanism of Limnos, Greece: Implications for the geodynamic evolution of the northern Aegean. *Contributions to Mineralogy and Petrology* **177**(8), 73.

Guillot S, Agbossoumondé Y, Bascou J, Berger J, Duclaux G, Hilairet N, Ménot R-P and Schwartz S (2019) Transition from subduction to collision recorded in the Pan-African arc complexes (Mali to Ghana). *Precambrian Research* **320**, 261–280.

Gunn P (1997) Regional magnetic and gravity responses of extensional sedimentary Basins. *AGSO Journal of Australian Geology and Geophysics* **17**(2), 115–131.

Hacker BR, Kelemen PB and Behn MD (2015) Continental lower crust. In *Annual review, Earth Planet Science* (eds R Jeanloz and KH Freeman), vol. 43, pp. 167–205.

Johnson TE, Fischer S and White RW (2013) Field and petrographic evidence for partial melting of TTG gneisses from the central region of the mainland Lewisian complex, NW Scotland. *Journal of the Geological Society* **170**(2), 319–326.

Kalsbeek F, Affaton P, Ekwueme B, Frei R and Thrane K (2012) Geochronology of granitoid and metasedimentary rocks from Togo and Bénin, West Africa: comparisons with NE Brazil. *Precambrian Research* **196**, 218–233.

Kalsbeek F, Frei D, Schersten A, Frei R, Gerdes A and Kalvig P (2020) Enigmatic 1146±4 Ma old granite in the southeastern rim of the West African craton, now part of the Dahomeyan orogenic belt in Ghana. *Journal of African Earth Science*, 103814.

Kelemen PB, Hanghoj K and Greene AR (2014) One view of the geochemistry of subduction-related magmatic arcs, with an emphasis on primitive andesite and lower crust. *Treatise on Geochemistry* **4**, 749–805.

Kornprobst J (2002) *Metamorphic Rocks and their Geodynamic Significance. A Petrological Handbook*. Dordrecht: Kluwer Academic Publishers.

Kwayisi D, Agra NA, Dampare SB, Asiedu DK, Amponsah PO and Nude PM (2017) Two Suites of gabbro in the Buem Structural unit, Southeastern Ghana: Constraints from new field and geochemical data. *Journal of African Earth Sciences* **129**, 45–55.

Kwayisi D, Elburg M and Lehmann J (2022a) Preserved ancient oceanic lithosphere within the Buem structural unit at the eastern margin of the West African Craton. *Lithos* **410**, 106585.

Kwayisi D, Lehmann J and Elburg M (2020) The architecture of the Buem Structural Unit: Implications for the tectonic evolution of the Pan-African Dahomeyide Orogen, West Africa. *Precambrian Research* **338**, 105568.

Kwayisi D, Lehmann J and Elburg M (2022b) Provenance and depositional setting of the Buem structural unit (Ghana): implications for the paleogeographic reconstruction of the West African and Amazonian cratons in Rodinia. *Gondwana Research* **109**, 183–204. https://doi.org/10.1016/j.gr.2022.04.020.

Liégeois J-P, Navez J, Hertogen J and Black R (1998) Contrasting origin of post-collisional high-K calc-alkaline and shoshonitic versus alkaline and peralkaline granitoids. The use of sliding normalization. *Lithos* **45**, 1–28.

Lu Y-J, McCuaig TC, Li Z-X, Jourdan F, Hart CJR, Hou Z-Q and Tang S-H (2015) Paleogene post-collisional lamprophyres in western Yunnan, western Yangtze craton: ante source and tectonic implications. *Lithos* **233**, 139–161.

Maniar PD and Piccoli PM (1989) Tectonic discrimination of granitoids. *Geological society of America bulletin* **101**(5), 635–643.

Milligan PR and Gunn PJ (1997) Enhancement and presentation of airborne geophysical data. *AGSO Journal of Australian Geology and Geophysics* **17**, 63–75.

Nude PM (1995) Petrology of selected migmatites within the acid belt of the Dahomeyan in southeastern Ghana. *MPhil thesis*. University of Ghana, Department of Geology, p. 103.

O'Connor JT (1965) A classification for quartz-rich igneous rocks based on feldspar ratios. *US Geological Survey, Professional Papers* 525B, B79–B84.

Opare-Addo E, Browning P and John BE (1993) Pressure-Temperature constraints on the evolution of an early Proterozoic plutonic suite in southern Ghana, West Africa. *Journal of African Earth Sciences (and the Middle East)* **17**(1), 13–22.

Oruc B and Selim H (2011) Interpretation of magnetic data in the Sinop area of Mid Black Sea, Turkey, using tilt derivative, Euler deconvolution, and discrete wavelet transform. *Journal of Applied Geophysics* **74**, 194–204. https://doi.org/10.1016/j.jappgeo.2011.05.007.

Paine JW (1986) A comparison of methods for approximating the vertical gradient of one-dimensional magnetic field data. *Geophysics* **51** (9), 1725–1735.

Palme H and O'Neill HS (2014) Cosmochemical estimates of mantle composition. In *Treatise on Geochemistry*, pp. 1–39. Oxford: Elsevier-Pergamon.

Pearce JA (2008) Geochemical fingerprinting of oceanic basalts with applications to ophiolite classification and the search for Archean oceanic crust. *Lithos* **100**(1-4), 14–48.

Pearce JA, Harris NB and Tindle AG (1984) Trace element discrimination diagrams for the tectonic interpretation of granitic rocks. *Journal of Petrology* **25**(4), 956–983.

Peccerillo A and Taylor SR (1976) Geochemistry of Eocene calc-alkaline volcanic rocks from the Kastamonu area, northern Turkey. *Contributions to Mineralogy and Petrology* **58**, 63–81.

Rollinson H (1993). Using geochemical data. *Evaluation, Presentation, Interpretation* **1**, 23–89.

Rudnick RL and Gao S (2014) Composition of the continental crust. In *Treatise on Geochemistry (Second Edition)* (eds HD Holland & KK Turekian), pp. 1–421 51. Oxford: Elsevier-Pergamon.

Sawyer EW (1999) Criteria for the recognition of partial melting. *Physics and Chemistry of the Earth, Part A: Solid Earth and Geodesy* **24**(3), 269–279.

Spandler C and Pirard C (2013) Element recycling from subducting slabs to arc crust: a review. *Lithos* **170**, 208–223.

Tarney J (1977) Petrology, mineralogy, and geochemistry of the falkland plateau basement rocks, site 330, deep sea drilling project.

Thiéblemont D and Tégyey M (1994) Geochemical discrimination of differentiated magmatic rocks attesting to the variable origin and tectonic setting of calc-alkaline magmas. *Comptes Rendus De L Academie Des Sciences Serie II* **319**(1), 87–94.

Wang Q, Xu JF, Jian P, Bao ZW, Zhao ZH, Li CF, Xiong XL and Ma JL (2006) Petrogenesis of adakitic porphyries in an extensional tectonic setting, Dexing, South China: implications for the genesis of porphyry copper mineralization. *Journal of Petrology* **47**, 119–144.

Whitney DL and Evans BW (2010) Abbreviations for names of rock-forming minerals. *American Mineralogist* **95**, 2010.

Winter JD (2001) *An Introduction to Igneous and Metamorphic Petrology*. Hoboken, NJ: Prentice Hall.

https://doi.org/10.1017/S0016756823000808 Published online by Cambridge University Press